
TOWARDS THE GENERATION OF SYNTHETIC IMAGES OF PALM VEIN PATTERNS: A REVIEW

Edwin H. Salazar-Jurado 

Doctorado en Modelamiento Matemático Aplicado

Universidad Católica del Maule

Talca 3480112, Chile

edwin.salazar@alu.ucm.cl

Ruber Hernández-García 

Laboratory of Technological Research in Pattern Recognition

Research Center for Advanced Studies of Maule

Universidad Católica del Maule

Talca 3480112, Chile

rfernandez@ucm.cl

Karina Vilches-Ponce 

Faculty of Basic Sciences

Universidad Católica del Maule

Talca 3480112, Chile

kvilches@ucm.cl

Ricardo J. Barrientos 

Laboratory of Technological Research in Pattern Recognition

Faculty of Engineering Sciences

Universidad Católica del Maule

Talca 3480112, Chile

rbarrientos@ucm.cl

Marco Mora 

Laboratory of Technological Research in Pattern Recognition

Faculty of Engineering Sciences

Universidad Católica del Maule

Talca 3480112, Chile

mmora@ucm.cl

Gaurav Jaswal 

Department of Electrical Engineering

Indian Institute of Technology Delhi

New Delhi 110016, India

gauravjaswal@iitd.ac.in

ABSTRACT

With the recent success of computer vision and deep learning, remarkable progress has been achieved on automatic personal recognition using vein biometrics. However, collecting large-scale real-world training data for palm vein recognition has turned out to be challenging, mainly due to the noise and irregular variations included at the time of acquisition. Meanwhile, existing palm vein recognition datasets are usually collected under near-infrared light, lacking detailed annotations on attributes (e.g., pose), so the influences of different attributes on vein recognition have been poorly investigated. Therefore, this paper examines the suitability of synthetic vein images generated to compensate for the urgent lack of publicly available large-scale datasets. Firstly, we present an overview of recent research progress of palm vein recognition, from the basic background knowledge to vein anatomical structure, data acquisition, public database, and quality assessment procedures. Then, we focus on the state-of-the-art methods that have allowed the generation of vascular structures for biometric purposes and the modeling of biological networks with their respective application domains. In addition, we review the existing research on the generation of style transfer and biological nature-based synthetic palm vein images algorithms. Afterward, we formalize a general flowchart for the creation of a synthetic database comparing real palm vein images and generated synthetic samples to obtain some understanding into the development of the realistic vein imaging system. Ultimately, we conclude by

discussing the challenges, insights, and future perspectives in generating synthetic palm vein images for further works.

Keywords Biometrics · Image synthesis · Palm vein recognition · Palm vein datasets · Synthetic palm vein images

1 Introduction

Biometric systems are very important in the modern era due to the increasing demand for security, using biology and technology to identify people around the world [1]. Therefore, physiological and behavioral traits with properties such as universality, distinctiveness, permanence, and acceptability are used in the identification process [1, 2]. The most commonly used characteristics are the fingerprint, iris, and face; however, they have limitations due to their exposure to the environment, making them susceptible to forgery. In contrast, more recent traits such as palm and finger veins are difficult to forge because they are not visible to the human eye [3, 4].

Palm veins become visible due to the hemoglobin in the blood plasma. For this purpose, a light array is used whose wavelengths are in the near-infrared spectrum. Thus, part of the light is absorbed by the hemoglobin, reducing the reflection range and producing gray patterns in the images, which corresponds to the vascular structures [5, 6, 7]. There are two methods for the acquisition of palm vein images: reflection and transmission. In the reflection method, the illumination component and the capture sensor are on the same side; these devices are low-cost and widely used in research [8, 9, 10, 11]. Whereas in the transmission method, the illumination array and the capturing sensor are on opposite sides. Hence, the lighting intensity must be of a high magnitude to pass through the tissues and muscles of the hand, which makes the device costly [2].

Most publicly available databases use the reflection method for image acquisition. However, in the database acquisition process, there are limitations in terms of time, security, and cost, which have raised challenges to explore this technology for large-scale applications [12]. Generally, research in palm vein biometrics has been focused on verification through data augmentation per subject rather than identification since publicly available databases have a reduced number of individuals and samples, as shown in Table 3. Thus, it is not feasible to evaluate the scalability of developed systems on massive datasets. In other biometrics such as fingerprints, handprints, or iris, the construction of large-scale synthetic databases has permitted the development of the corresponding biometric technologies. Hence, synthetic database generation allows to rapidly progress in the research field while preserving the security of users and also proving to be inexpensive compared to the traditional collection of biometric samples [13, 14, 15, 16].

Regarding the image generation of vascular structures for biometric recognition, according to our literature review, there are only two approaches focused on palm vein imaging to produce synthetic ROI samples of palm vein images [17, 18]. Both works mark a milestone by preliminary validating and introducing two different synthetic palm vein databases, which are the largest of the state-of-the-art. However, the proposed methods are based on two generalist techniques that do not explicitly consider the topology of the palm vascular system. Moreover, other studies have provided methodologies for the generation of synthetic vein images such as dorsal hand veins [13], finger-vein images [4, 19, 20], and sclera vascular network [21]. However, it could be argued that the simulation of palm vein patterns is a difficult task due to the complex vein structures of the hand [22, 23]. In fact, the different movements of the hand require many structures working synchronously, organizing multiple vessel networks to ensure a constant blood flow.

In real images, vascular network analysis is performed using various segmentation techniques [24, 25]. Particularly in [24], the methods are divided into six categories: pattern recognition techniques, model-based approaches, tracking-based approaches, artificial intelligence-based approaches, neural network-based approaches, and tube-like object detection approaches. The difference of each method lies in the ability to extract the venous pattern from the images, sharing the disadvantage that they are not robust to low-quality images, which prevents a detailed characterization of the vascular structure of the palm. Despite the above, methodologies associated with the study of different biological networks found in nature can be used to simulate the palmar venous structure. These networks have shown certain similarities with blood networks that allow their comparison [26, 27, 28, 29, 30]. Particularly, any biological network is formed by a hierarchical network composed of primary veins with branches into lower-order veins. These branches may have a free termination, producing an open venation pattern, or they may be connected by anastomosis, forming loops in a closed shape [29]. Biological network modeling involves both phenomenological and qualitative parameters, such as allometric scaling laws and geometry, respectively. Besides, growth rules can be expressed by differential equations (ordinary or partial) or by computational modeling.

Extensive experimental work has been published in the literature to formulate models for the formation and growth of vein networks [27, 31, 32]. In [27], the authors reviewed the mathematical models for vascular networks formation, which are based on two main mechanisms: vasculogenesis and angiogenesis. Their work emphasizes the ability to reproduce different biological systems and predict measurable quantities describing the overall processes. Additionally,

a survey of mechanistic-based plant modeling techniques that approach plant morphogenesis from geometric and molecular perspectives is presented in [31]. On the other hand, the authors of [32] study modeling techniques for reconstructing blood vessels from brain images; the related models are classified into three categories: image-based modeling, mathematical methods, and hybrid models. According to their analysis, image-based modeling consists of pre-processing and feature extraction techniques, mathematical methods produce characteristics of the vascular network, and hybrid models are a fusion of the two methods.

Contrary to previous works, the present work allows establishing state-of-the-art approaches for the generation of vascular networks to deepen knowledge towards the synthesis of palm vein images. Our objective is to determine their applicability for the simulation of different structures associated with the palm vein patterns. Additionally, we include models of networks that have been used for other purposes, such as aggregation methods that arise in non-organic environments and adaptive dynamics methods that govern the behavior of some multi-cellular organisms. Moreover, it should be noted that the works reported in the literature have focused on the generation of network structures, which only represent a single characteristic associated with the distribution of real palm vein images. However, for the generation of synthetic palm vein images with biometric purposes, it is also required to consider qualitative parameters associated with the structure, texture, illumination, and contrast. These factors are also reviewed in this paper by establishing the parameters that influence the visualization of vascular patterns. Besides, we introduce a general flowchart for creating large-scale synthetic databases of palm vein images to obtain some understanding into the development of the realistic vein imaging system.

Accordingly, the contributions of our study are as follows:

- An analysis of the factors that affect the visualization of vascular structures on images, aiming to outline the parameters that must be taken into account in the development of mathematical or computational models for the generation of synthetic palm vein images, including the vein anatomical structure, the acquisition of palm vein images, quality assessment procedures, and public palm vein databases.
- An extensive study on the existing approaches to model vascular networks determining their applicability to produce different vein patterns that could be used to generate palm vein images.
- A general scheme for the creation of large-scale databases of synthetic palm vein images comparing real palm vein images and generated synthetic samples to obtain some understanding into the development of the realistic vein imaging system. Using this scheme, we increased the size of the proposed databases in [17] and [18], which are the largest datasets of the state-of-the-art facilitating the evaluation of large-scale biometric methods based on palm vein recognition. Moreover, the proposed scheme for image generation is incremental that allows increasing the number of individuals in the databases continuously.
- An overview on the main challenges, insights, and potential future research directions for the development of synthetic palm vein databases for further studies.

The rest of the paper is structured as follows. Firstly, Section 2 provides an overview of the processes involved in the visualization of palm veins, emphasizing on the vascular structure of the palm, the image acquisition process, and methods for evaluating image quality. A discussion of public palm vein databases for person recognition is given in Section 3. Then, Section 4 reviews state-of-the-art approaches that provides a conceptual basis for generating synthetic images of palm veins. Later, Section 5 introduces a general scheme for the creation of a synthetic database and evaluates two generalist methods for palm vein imaging. Finally, sections 6 and 7 conclude our work by analyzing the main challenges and perspectives for further investigations on the generation of synthetic palm vein images.

2 Background Knowledge on Palm Vein Images for Biometric Recognition

A palm vein-based recognition system can be summarized into four main processes [2]: (1) image acquisition; (2) pre-processing for image segmentation and enhancement; (3) feature extraction; and (4) recognition process. Compared to other traditional biometric techniques such as fingerprint, iris, or face, the palm vein pattern as a biometric trait is relatively new; thus, there are still several challenges to study. Particularly, studying the vascular networks of the palm and the image acquisition process is essential in order to create synthetic palm vein images, which is the main aim of the present research.

2.1 Vascular Network of the Hand

The vascular networks of the hand are divided into veins and arteries. The veins drain deoxidized hemoglobin (Hb), and the arteries transport oxidized hemoglobin (HbO_2). The vascular anatomy of the palm and its functional aesthetic units are represented in Figure 1, where a distinction is made between deep and superficial branches with various connections

between these two sets [33]. The superficial veins are located immediately below the epidermis and between the two superficial fasciae, as can be detailed in the circular zoom of Figure 1.

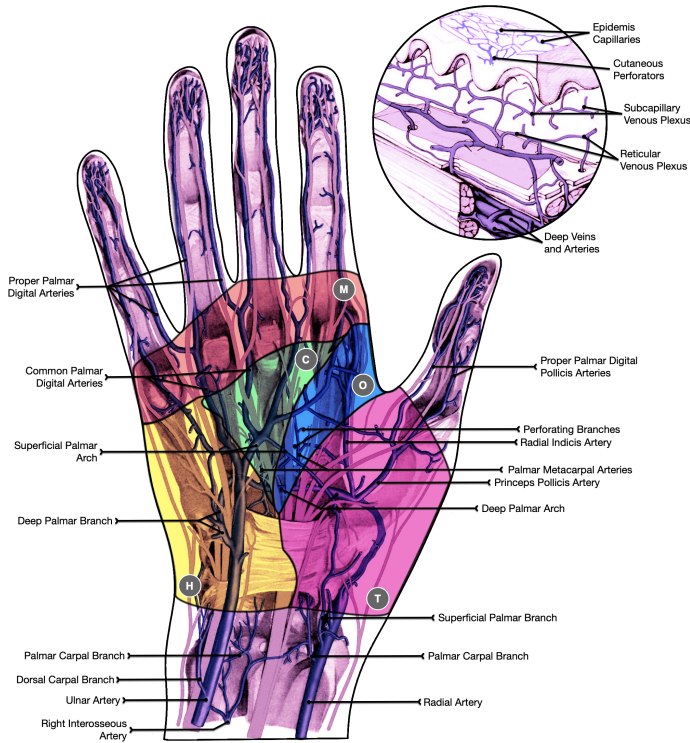


Figure 1: Representation of the vascular anatomy of the palm and functional aesthetic units: Thenar (T), Opposition (O), Hypothenar (H), Central triangular (C), and Metacarpal (M). The circular zoom shows the organization of the vascular structures inside the skin.

The vascular structure of the palm shows complex patterns that ensure unobstructed blood flow when any movement of the hand occurs [34]. These patterns are precisely those that allow the vascular network to be a biometric trait for identification, of which superficial networks are mainly used due to the optical limitations of acquisition systems. [13]. There is a classic description of the superficial arterial topology of the palm, as shown in Figure 1. A superficial palmar arch around the metacarpal bones arises from the anastomosis of the ulnar artery with the radial artery and branches into the common palmar digital arteries. In the top of the palm, where these arteries reach the proximal phalanges, they branch into palmar digital arteries to supply blood to the fingers [35].

In addition to the classic structure mentioned above, there are some variants with the same relevance. According to different studies [36, 37, 38], the typical case corresponds to only 55% or less of the analyzed patients. Specifically, in [38] they classified 86 hands according to the absence of the palmar arch or according to the anastomosis of the arteries, as shown in Figure 2. In the case of the absence of the arch, the structure may form two configurations: irrigation produced solely by the ulnar artery (Dominant Ulnar) or by two arteries independently (Codominant). The first structure was found in 29% of the samples, of which 6% presented a small radiopalmar artery that ends at the level of the thenar muscles (Ulnar/Radiopalmar (Thenar) Pattern). The second case was reported in 13%, including 8% showed a structure formed by the ulnar and the radial artery, and 5% comprised of the ulnar and medial arteries.

Regarding the anastomosis of the arteries that form the palmar arch, it can occur in two forms [38]: the arteries forming the arch are in the same plane, or the radial artery passes through the lower part of the muscle to anastomize with the ulnar artery. In the first case, the structure was present in 43% of the samples; 22% corresponds to the classic case and 21% to a variant, where the radial artery participates to a lesser extent in the arch formation (Ulnar pattern). The second case is less usual, where the network pattern only appears in 15%; of which 7% with a structure similar to the classic case, and the remaining 8% is like the Ulnar pattern, the difference lies in the fact that the radial artery passes through the lower part of the muscle.

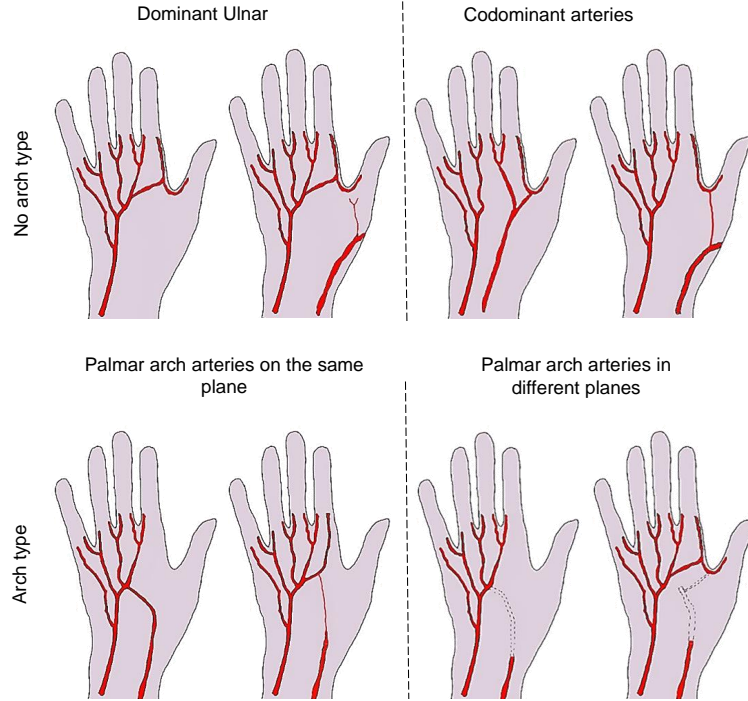


Figure 2: Structure variants of the palmar arch, based on the classification proposed in [38].

On the other hand, the topology of palm veins is a less studied topic, paying more attention to their functionality; in particular, how veins can avoid compression during grasping is studied [39]. Although the structure of palm veins is unknown, research in plastic surgery has provided information about the blood supply in the skin, allowing classification of the complex vascular pathways by direct cutaneous perforator vessels and indirect cutaneous vessels [40, 41]. The former arises from the underlying veins and pass between muscles and other structures and then perforate the outer layer of the fascia where their primary destination is the skin, as shown in the zoom of Figure 1. In contrast, indirect cutaneous vessels penetrate the deep tissues vertically or obliquely before perforating the outer layer of the fascia, which may emerge as small terminal branches to provide secondary supply to the skin.

Furthermore, for the location of the different perforator veins of the palm it is determined based on their five functional regions [42]: Thenar (T), Opposition (O), Hypothenar (H), Central triangular (C), and Metacarpal (M), as highlighted with different colors in Figure 1. Thus, it is assumed that the direct perforants are located in the articulation of each of the regions, and the indirect perforators are within the functional regions. Therefore, each perforator forms an angiosomal module defined by a perimeter of anastomotic vessels that connect it to its neighbor in all directions. [41]. The size and length of the cutaneous perforators may vary, but they all interconnect to form a network of vessels. These are well developed in the dermis, the sub-dermis, the subcutaneous's lower surface, and the deep fascia's outer surface.

2.2 Acquisition of Palm Vein Images

The acquisition of palm vein images is carried out using near-infrared (NIR) devices that interact with oxidized hemoglobin (HbO_2) and deoxidized hemoglobin (Hb) in the vascular network [2]. Figure 3 depicts the penetration depth and path of the light into the skin and the corresponding absorption coefficients of HbO_2 , Hb, and water. The optical window from 720nm to 950nm used for image acquisition is highlighted. When the light wavelength is between 720nm and 760nm, the radiation is strongly absorbed by Hb, producing a shadow corresponding to the vein pattern. At 790nm, there is an intersection point where Hb and HbO_2 present the same absorption, which allows the visualization of veins and arteries. Meanwhile, for higher spectral ranges of the optical window HbO_2 presents a slight increase compared to Hb.

The different absorption rates of NIR radiation make it possible to identify the location of veins and arteries while minimizing the influence of the surrounding tissue. It is worth mentioning that the amount of optical penetration depth ranges from 0.5 to 5mm due to reflection, scattering, or fluorescence phenomena occurring in the different tissues of the palm, as shown in Figure 3. Consequently, vein acquisition devices can only capture superficial veins [43]. The

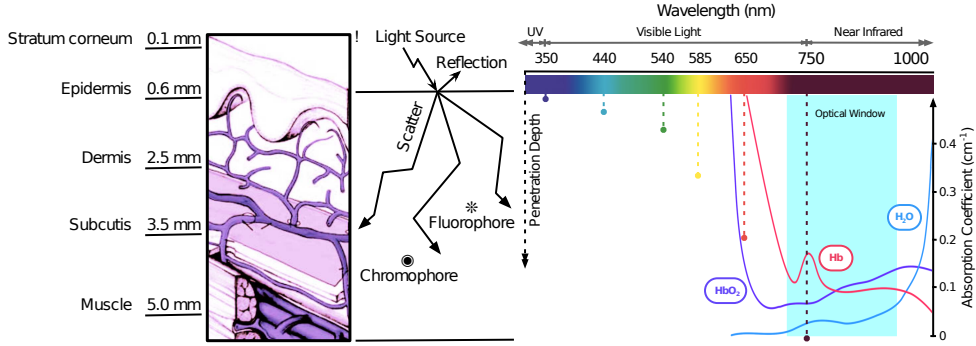


Figure 3: Penetration depth and path of the light into the skin, for different wavelengths and the corresponding absorption coefficients of oxidized hemoglobin (HbO_2), deoxidized hemoglobin (Hb), and water (H_2O).

resulting visualization of palm vein patterns in captured images depends on many variables. Figure 4 summarizes a classification of these parameters based on three groups: soft biometrics, local contrast, and illumination conditions.

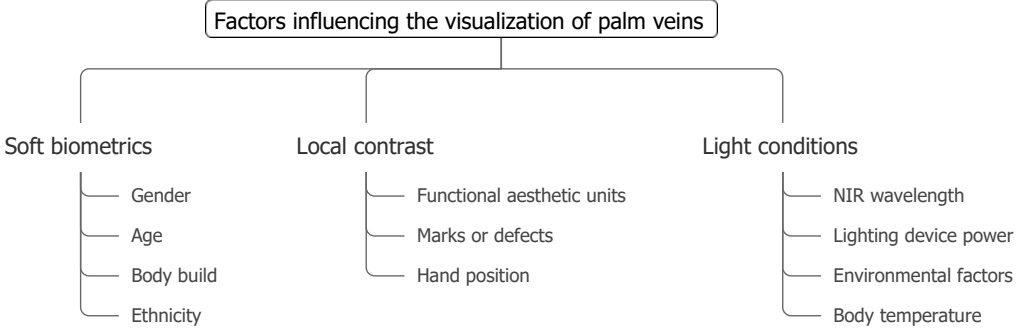


Figure 4: Classification of parameters that produce variability in the visualization of palm vein patterns in captured images.

The first group of variables is related to soft biometrics, which can modify the brightness and contrast of palm vein images, such as gender, age, body build, and ethnicity. Gender can be differentiated by palm color and texture [44, 45]. The male palm generally shows a darker partial shade and more textural differences resulting from the greater grip. Furthermore, in [46] it is studied the features associated with vein topology, such as the gradient of the vein pattern, providing information about gender. On the other hand, the individual's age and body build affect the elicitation of the venous pattern of the palm, as the light intensity varies due to different hemoglobin and water levels in the veins and skin. The last parameter considered in this category is ethnicity since images may depend on skin tone. Particularly, in [47] it is studied the influence of near-infrared radiation on backgrounds of different colors. In some cases, background absorption dominates the spectra and reduces the spectral characteristics of hemoglobin. Associated with that, it is worth mentioning that only the VERA database [48] collects extra information about the sex and age of the individuals. Due to the characteristics of the participants, as shown in Figure 6, it can be noted that the representativeness of some groups is limited, which reduces the performance of gender and age classification based on palm vein images [46, 49] and limits the study of these factors on the variability of the image.

In addition, some variables influence the local contrast, such as the functional aesthetic units of the palm, palmprint marks or defects, and the position of the hand in the acquisition device. These parameters generate regions with different levels of contrast and light intensity. The brightness and contrast in the fingers are the closest to the study of light variation in different palm regions. In [50], it is shown that identification results are improved using the proximal part of the finger rather than the distal part. Additionally, authors of [4] simulate the illumination effects that occur in some regions of the finger. Particularly, they focused on the interphalangeal joints since a higher light penetration through the finger occurs because the fluid has a lower density than the bones. In the case of the palm, we can distinguish five functional regions, as shown in Figure 1, which produce variations in relief and brightness in the images. This effect can be observed in the images of public datasets presented in Figure 5, where a lower density of veins in the central regions (Opposition (O) and Central triangular (C)) can be noticed. As for the marks and defects in the palmprint being visible

in the image inevitably lead to poor visibility of the vein patterns [51]. However, scars are skin markings that have a geometric distribution contributing to the identification of individuals [52]. The last parameter considered concerning local contrast is the hand position, which causes geometric and perspective variations due to inconsistent positions and postures of the hands with respect to the camera [53]. It is worth noting that [54] shows that tilting, bending, planar and nonplanar rotations cause severe performance degradations of publicly available datasets.

On the other hand, the illumination system is one of the most critical aspects of the image acquisition process, involving NIR wavelengths and the power of the illumination device. The NIR wavelength influences the visualization of vein patterns because of the irregularity in the absorption of hemoglobin and other tissues [50]. Some wavelengths in the near-infrared spectrum range are more capable of acquiring biometric traits than others, as shown in multispectral databases such as CASIA [55] and PolyU [56]. Furthermore, the power of the illumination device must ensure uniformity and avoid over-saturation of the captured image. To regulate the illumination power, multiple layers of diffusers and different LED configurations have been used to modify the intensity distribution, mainly when the camera must be located on the same side as the light source [57]. While high power light sources have the undesirable effect of decreasing contrast due to a large amount of radiation emitted, in contrast, low-intensity light sources are not able to penetrate the skin tissue, not allowing visualization of the vein pattern [58]. Besides, two external parameters influence the lighting conditions, namely environmental factors and body temperature. Environmental factors such as temperature and surrounding illumination can lead to unstable gray value distribution patterns in images [59]. These factors acquire greater relevance when far-infrared spectroscopy techniques are used. [60]. Finally, body temperature is an important component of vasodilation that increases heat loss and blood flow at the palm surface, resulting in darker images [61].

In summary, palm vein images are affected mainly because the acquisition devices are faced with uncontrolled parameters such as uneven illumination and hand position. Additionally, they are affected by device-independent parameters related to soft biometrics and lack of robustness due to outdoor illumination [62, 19]. To deal with the above, different acquisition devices have been proposed. Table 1 summarizes the proposed acquisition devices for palm vein imaging that change depending on the sensor type, illumination method or mounting, and hardware components, resulting in a large variety of images that cannot be compared because of the non-standardization of the method. There are some techniques to evaluate the quality of palm vein images; however, these are also not standardized [2]. Therefore, considering that image quality is a key predictor in the biometric recognition process [63], it would also allow a comparison between real and synthetic databases. The following section describes the proposed procedures for evaluating the quality of vein images.

2.3 Image Quality of Palm Vein Images

From a general perspective, the quality assessment of infrared images has been performed mainly by human inspection using the National Imagery Interpretability Rating Scale (NIIRS) standard [69]. The aspects involved in image interpretability are resolution, contrast, and edge sharpness. For biometric images such as fingerprints, iris, and face, there is the ISO/IEC 29794 standard [70, 71, 72] that takes into account geometric and posture aspects. Particularly, for palm vein recognition as a contactless biometric system, the image quality greatly reduces the identification performance. However, in the case of vascular-based biometrics, there is still no standardization that provides a metric to assess the image quality [2]. Consequently, each research related to the quality of palm vein imaging uses self-created metrics leading to the respective quality scores. To the best of our knowledge, Table 2 summarizes the published studies in this area, which have been limited to working with self-constructed images. Following, we describe the main characteristics of each work.

In [63], a device for acquiring high-quality images of palm veins is proposed to avoid the low quality of captured images. The quality of the images is evaluated using the 2D image entropy and the local 2D entropy. The calculation is performed by the accelerated implementation method using Field Programmable Gate Array (FPGA) platform. The acquisition device controls the intensity of the NIR light source and camera parameters based on the image quality. Therefore, taking into account the quality of the resulting image, the device recaptures the image until a high-quality image is obtained.

On the other hand, the authors of [73] evaluated the image quality as a function of the distance between the palm to the camera lens. The paper studies the relation between distance and recognition performance based on the image quality evaluation. The proposed evaluation method consists of two parts: (1) analyzing the detail change from the image clarity and (2) examining the structural difference of the image. The first part is performed through the Tenengrad energy gradient function, which uses the Sobel operator to extract the horizontal and vertical gradient values. The second part is performed by using the SSIM structural difference method [77], which is calculated as a function of light, structure, and contrast. Although this work shows that the image quality depends on the distance from the palm to the camera, they do not specify the ranges in which the image quality oscillates. Besides, their results determine an adequate distance range for the acquisition of the vein pattern; outside these values, the false rejection rate increases.

Table 1: Summary of acquisition devices for palm vein imaging.

Sensor Type	Method and NIRline Spectrum	Hardware andline Components	Contactless Device	Pros and Cons
Multispectral CCD line Camera [55]	Multispectral Reflection (460nm, 630nm, 700nm, 850nm, 940nm, VIS)	Infrared LEDsline (violet to IR), optical diffusers	Yes	The recognition is performed both with the palm print and the internal structures. However, the vein pattern is barely visible.
ImagingSource Sony ICX618 [48]	Reflection (940nm)	HC-SR04 ultrasound sensor and a led signal (palm position)	Yes	The system is sensitive to the position of the hands, sometimes generating blurring images.
USBline camera [64]	Reflection (880nm)	Infrared LEDs (880 nm), LED diffusers	No	It is a contact acquisition device, which allows controlling the illumination conditions to obtain a better vein pattern. However, it reduces the level of hygiene.
Multispectral CCDline Camera [56]	Multispectral Reflection (470nm, 525nm, 660nm, 880nm)	Multispectral light, standard closed-circuit television camera, light controller, monochromatic CCD	No	The multispectral range allows highlighting different texture information of the palm. However, it is not clear how to best merge multispectral information.
CCDline camera [58]	Reflection (940nm)	Ring near infrared LED light source, a power regulator, LCD with a touch screen	Yes	It is possible to adjust the illumination power and determine the palm position on the LCD screen to obtain a good image. However, the device has the disadvantage that it is not automated.
USB camera mvBluefox IGC [62]	Reflection (NIR array 850nm and 940nm)	Infrared LEDs array (850nm and 940nm)	Yes	Infrared LEDs were placed alternately. Three arrays of LEDs were used: two of them to illuminate the hand, and the third to illuminate the fingers. The finger-vein information can improve the performance of the palm vein recognition.
Adaptedline web-cam [65]	Multispectral Reflection (VIS, 700nm, Thermal)	Thermal camera, webcam, filters for IR, infrared LEDs	No	The device allows the capture of 3 images: in the visible spectrum (VIS), IR spectrum, and thermal. The results show that VIS images provide the best identification rates. The above indicates that the IR setup is not of good quality.
CMOSline camera [66]	Reflection (IR)	Camera with adjustable support (360° rotation in the plane of the palm) and wooden hand guides	No	CMOS sensors employ a smaller digital circuit that uses less power and are less expensive than other devices. However, the images produced have lower visual quality.
Adaptedline web-cam [67]	Reflectionline (900nm to 920nm)	Infrared LEDs (880nm to 920 nm), optical diffusers	Yes	The user is not restricted to a particular position because the image is saved as a real-time video sequence at 30 fps. However, the storage device may require a lot of memory
CCD camera [68]	Reflection (850nm)	Concentric LED arrays, holographic diffusers, lighting control system	No	The diffuser scatters the light diminishing the radiation intensity.

Subsequently, Wang *et al.* [74] introduced an algorithm to evaluate the quality of palm vein images based on the tilt angle of the hand and a fusion of two criteria, namely clarity and brightness uniformity. The image clarity is estimated based on the method developed in [78], by performing discrimination between different levels of image blurring. On the other hand, the brightness uniformity is computed by averaging the gray difference between different parts of the palm vein image. Both criteria are combined by using a weighted quality score in the range [0..1], where 1 corresponds to the best quality image. The evaluation of the proposed algorithm was performed on 60 images of different individuals by varying the tilt angle and blurring from the same person's hand. Finally, they found that the image quality decreases as the tilt angle increases; meanwhile, it is less sensitive to brightness uniformity. In their experiments, the quality score ranged from 0.446 to 0.543. However, it should be noted that more extensive experimentation should be conducted.

Moreover, Dong *et al.* [75] designed a multi-spectral adaptive device to examine the image quality as a function of light source intensity. The proposed capturing system allows adjusting three light source wavelengths (760nm, 850nm, and 940nm) and then collecting the high-quality palm vein image. The image quality index is calculated by integral scores from the mass fractions of mean and variance gray levels. Their analysis of experimental results showed that variations of illumination power produce images with different qualities, ranging from 0.3 to 0.8. The overall evaluation range is [0..1], where 1 represents the best quality. As in previously discussed works, the conducted experimental assessment is quite preliminary.

Lastly, to our best knowledge, the most complete work reported is [76]. Authors propose a methodology to evaluate palm vein image quality based on statistics of natural scenes and reject poor-quality images. In this way, the image quality is the result of three quantitative measures. The first proposed measure computes the difference between the minimum and the maximum gray mean to estimate the brightness uniformity among several image patches. Secondly, statistics of pixel intensities are calculated by using the natural image quality evaluator (NIQE) method proposed in [79]. For the last metric, statistics of four kinds of Harr-Like features are computed by using natural scene statistics and the Mahalanobis distance. The overall image quality score is equal to the brightness uniformity score times a linear combination of the other two measures. The evaluation of the algorithm was performed on 60 self-captured images from 21 individuals. Experimental results show the effect of uneven illumination due to different tilt angles of the palm

Table 2: Reported studies on the image quality assessment of palm vein images. Evaluation range, lowest and highest scores are from the referenced papers; N/A means "not applied" or "not reported".

Method	Parameters of the acquisition system	Evaluation parameters	Evaluation range	Lowest score	Highest score
High quality palm vein image acquisition [63]	Intensity of NIR light source and camera parameters	2D image entropy and local 2D entropy	N/A	N/A	N/A
Image quality and recognition with different distance <i>et al.</i> [73]	Distance to the camera lens	Image clarity, image structural difference, and match results	0 – 1	N/A	N/A
Image quality assessment based on tilt angle [74]	Tilt angle of the palm (0° – 50° , with step of 10°)	Clarity and brightness uniformity	0 – 1	0.446	0.543
Multi-spectral adaptive capturing system based on image quality [75]	Intensity of the multi-spectral light source	Mean and variance of gray levels	0 – 1	0.3	0.8
Palm vein image quality assessment by using natural scene statistics features [76]	Tilt angle of the palm (0° – 50° , with step of 10°)	Illumination uniformity, natural image quality evaluator (NIQE), and statistics of Harr-Like features	N/A	4.190	1.622
GLCM metrics [67]	N/A	Threshold of acceptance as a function of contrast, variance, and correlation	N/A	N/A	N/A

and the quality scores for different distortion levels. The image quality as a function of hand position ranged from 4.190 to 1.622, and as a function of distortion ranged from 8.605 to 2.261, where the lower value corresponds to the best quality image. Despite this, the quality score is not bound in a closed range.

Furthermore, in order to broaden the scope of quality assessment methods of palm vein images, related works on finger-vein imaging have also been considered as the acquisition devices share many similarities [4]. In [80] they proposed an extension of the Peak-Signal-to-Noise (PSN) index that incorporates properties of the human visual system and measurements of finger-vein imaging such as finger area and displacement. Besides, Yin *et al.* [81] utilized the ability to filter out low-quality finger vein images. On the other hand, authors of [82] and [83] evaluated the image quality by employing the binary segmentation of vessel structure. The former method is based on support vector regression, and the latter one uses a CNN approach. As supervised learning methods, both approaches share the disadvantage of requiring a significant amount of labeled training data.

In our understanding, the evaluation of the quality of palm vein images has only been performed on self-captured images. Consequently, there are no common elements to compare quality between different public databases. Therefore, there is no evidence of intra-class and inter-class variability for the generation of synthetic palm vein image databases.

3 Publicly Available Datasets on Palm Vein Images

Among all the real-world applications, palm vein recognition has been adopted for authentication purposes in many kinds of public uses [84]. Fujitsu Labs provides a palm vein scanner and SDK for palm vein authentication, which reports a very low False Acceptance Rate (FAR) of 0.00008% and a False Rejection Rate of 0.01% [85]. In this context, Fujitsu conducted the most extensive research study on palm vein recognition with a database comprised of 75,000 subjects and a total of 150,000 palm vein images. However, their technology is private and patented, not allowing the use of captured palm vein images to evaluate different approaches or create public datasets of palm vein patterns for research purposes. Moreover, the study was conducted for commercial purposes, and the database is not available to reproduce the experiments or compare new approaches.

In this context, the research community has introduced some self-created databases of palm vein images [12], which have been collected by using self-designed and low-cost devices. As a result of the above, many non-standardized approaches use different collection protocols and different acquisition devices and equipment. Besides, these conditions produce different image parameters, variations in illumination and contrast, and also performance results. Table 3 provides an overview of the publicly available databases, comparing the number of subjects, captured hands and samples, acquisition sessions, total images, and their resolution. Additionally, Figure 5 shows image samples from each dataset.

As can be noticed in Table 3, public databases are usually composed of a limited number of people with no more than 300 individuals. Usually, the proposed approaches on palm vein recognition follow the *nom L&R* protocol from [48],

Table 3: Details of the publicly available databases of palm vein images. The number of subjects and the number of samples are expressed as Subjects \times Hands, and Samples \times Acquisition Sessions, respectively.

Database	Subjects	Samples	Total Images	Image Size	Sessions Interval	Labeling	Dataset Available
CASIA [55]	100 \times 2	3 \times 2	7,200	768 \times 576	30 days	Id	National Laboratory of Pattern Recognition (NLPR)
VERA [48]	110 \times 2	5 \times 2	2,200	480 \times 680	5 minutes	Id, Age, Gender	Idiap Research Institute
PUT [64]	50 \times 2	4 \times 3	1,200	1280 \times 960	7 days	Id	Poznan University of Technology
PolyU [56]	250 \times 2	6 \times 2	6,000	352 \times 288	9 days	Id	Biometrics Research and Innovation Centre (BRIC)
Tongji* [58]	300 \times 2	10 \times 2	12,000	800 \times 600	61 days	Id	By e-mail requesting
IITI* [62]	185 \times 2	6 \times 1	2,220	2592 \times 1944	N/A	Id	By e-mail requesting
Tecnocampus [65]	100 \times 2	2 \times 5	6,000	640 \times 480	28 days	Id	Signal Processing Laboratory (SPLab)
FYO [66]	160 \times 2	1 \times 2	640	800 \times 600	10 minutes	Id	Eastern Mediterranean University
Synthetic-sPVDB [17]	10,000	6 \times 1	60,000	128 \times 128	N/A	Id	LITRP Lab
NS-PVDB [18]	2,000	6 \times 1	12,000	128 \times 128	N/A	Id	LITRP Lab

*These datasets are publicly available by requesting to the principal investigator.

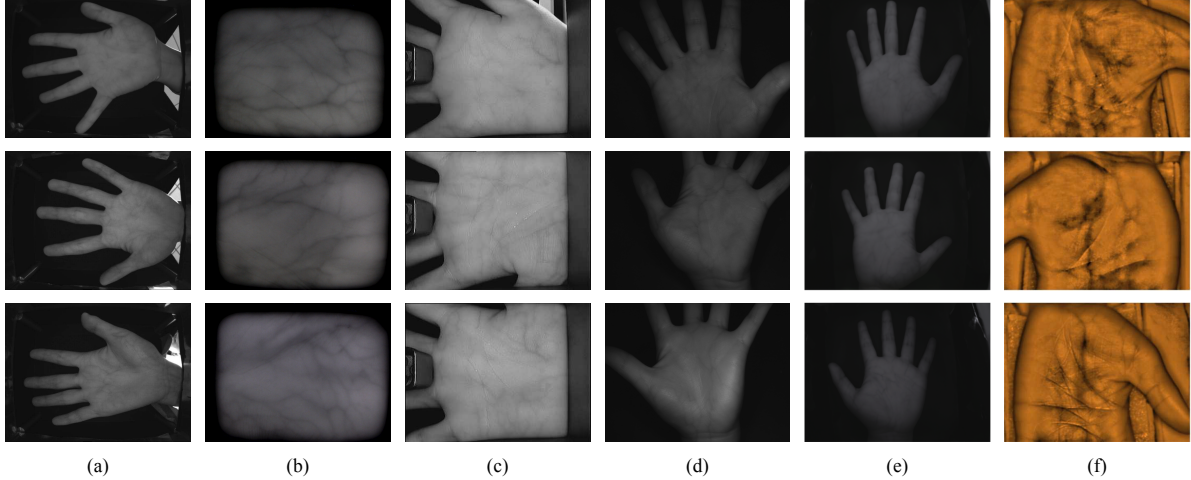


Figure 5: Exemplary of original palm vein samples from the public databases: (a) CASIA, (b) PUT, (c) PolyU, (d) Tongji, (e) IITI, and (f) FYO. Images from the VERA and Tecnocampus datasets are not shown due to restrictions of their terms of use.

where the left and right hands of the same subject are considered different subjects, doubling the number of subjects in the datasets. However, there is still a lack of increasing the number of individuals in the datasets to allow the study of scalability of the proposed methods for massive identification, i.e. at least up to a city population of hundreds of thousands to millions of people. A possible solution to address this drawback could be to use images from all databases, but this would not solve the problem because of two main reasons. First, only a total of 2,510 individuals would be obtained, which would still be insufficient to evaluate methods for massive recognition of people. Second, and most noteworthy, the characteristic variations of images resulting from different acquisition systems (e.g. resolution, illumination, contrast, etc.), as shown in Figure 5, may cause problems in training and parameter tuning of the proposed algorithms.

During the last years, the most recent approaches on palm vein recognition have focused on deep neural networks (DNN) (i.e. convolutional neural networks (CNN)), which are able to learn more robust feature representations. DNN-based methods have improved the state-of-the-art (SOTA) results on palm vein databases, achieving 100% of accuracy for four of eight public databases (i.e. Tongji [58], VERA [48], PolyU [56], and FYO [66]). However, DNN-based models have serious issues related to available training datasets, adjusting many parameters, scalability, among others. In this context, the small number of samples per class restricts the available training data for vein recognition tasks, which, at

the same time, reduces the generalization performance because DNN is highly dependent on the number of training samples. The above issues have motivated two main solutions: the use of pre-trained models and the application of data augmentation techniques or complex training processes for a task-specific network. Besides, it is important to note that the dataset partitions (i.e. training, validation, and testing) are not standardized, even among the existing approaches themselves [86], which limits the comparison of the proposed approaches.

Additionally, it is relevant to notice that only the VERA Palm vein dataset [48] includes additional labeling metadata such as gender and age. The database comprises 40 women and 70 men whose ages are between 18 and 60, with an average of 33 years old. Figure 6 shows the overall distribution of age and sex groups from the VERA database. It is noteworthy that there are significant differences between groups, lacking more representativeness of data to conduct deeper studies. The extra labeling metadata is a piece of valuable information because it is demonstrated that vein patterns are affected depending on some soft biometric traits such as gender, ethnicity, physiological composition, and medical conditions [44, 45, 46, 49, 87]. Thus, this auxiliary information can contribute to improving the accuracy of the recognition process.

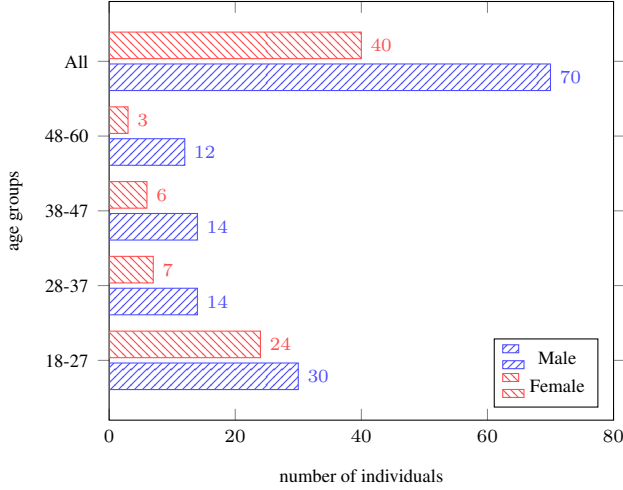


Figure 6: Overall distribution of age and sex groups from the VERA database.

To address the aforementioned limitations, some biometric techniques (e.g. fingerprint, iris, or face) have adopted the generation of synthetic databases. Particularly, synthetic images are very effective for evaluating the performance of several image processing algorithms, but their use for biometric purposes is a controversial issue. However, synthetic databases have the advantage of avoiding a time-consuming collection process and also do not compromise users' security at all, which is usually a personal concern regarding privacy violations [14, 15, 16]. Moreover, this kind of dataset does not entirely replace the validation with real images, whereas the generation of synthetic samples facilitates the validation of proposed approaches on large-scale databases.

Thereby, in our previous works [17, 18], we proposed two synthetic databases of palm vein images based on two generalist approaches. The first dataset, named Synthetic Style-based Palm Vein Database (Synthetic-sPVDB), comprises 10,000 individuals with six samples each, totaling 60,000 images. The generation method was implemented using the StyleGAN model [88]. The other dataset, called Natural-based Synthetic Palm Vein Database (NS-PVDB), was created using a procedure based on biological transport networks [89], being comprised of 12,000 images corresponding to 2,000 different subjects. The generated datasets are the largest in the state-of-the-art and were validated using qualitative and quantitative metrics to measure their similarities compared to the real images. As part of the present work, and taking into account the previous results, in Section 5 we present the formalization of a general flowchart for the generation of large-scale synthetic databases of palm vein images. Besides, we introduce larger versions of the proposed databases and extend experimental results in order to validate them.

Then, the present study aims to analyze and systematize the information available in the state-of-the-art regarding the generation of synthetic images of venous structures. Most studies in the literature related to the synthesis of the human vascular network have been oriented to medical purposes either to describe the growth of tumors or to diagnose diseases. On the other hand, within the biometric context and according to the bibliographic review, there are few works focused on providing methodologies for the generation of synthetic images for vein-based recognition, such as finger-vein [4], dorsal-hand [13], and sclera [21]. Hence, in the following sections, we review the most relevant

state-of-the-art approaches, discussing their advantages and disadvantages towards the challenging task of synthetic palm vein imaging for biometric purposes.

4 Review on the Generation of Synthetic Images of Vascular Networks Patterns

The lack of large-scale databases of vein patterns images has greatly limited the development of large-scale recognition methods that can be implemented for massive individuals identification [90, 91, 92]. In other biometric domains, such as fingerprints, have benefited from synthetic images that have avoided all issues concerning privacy regulations, allowing the rapid development of biometric technologies [12]. As for synthetic vein imaging, it faces issues such as low image quality and complex vascular patterns formed [39]. Aiming to deepen knowledge towards the synthesis of palm vein images, we review state-of-the-art models that have allowed the generation of vascular structures for biometric purposes and the modeling of biological networks with their respective applications.

4.1 Generation of Vein Networks Oriented to Biometric Recognition

To the best of our knowledge, there are few works focused on generating synthetic vein images for biometric purposes. Table 4 summarizes the reported approaches for different biometric purposes such as the synthesis of dorsal hand veins [13], finger-vein images [4, 19, 20], sclera vascular network [21], and the ROI of palm vein images [17, 18].

Table 4: Overview of state-of-the-art works on the generation of vein networks oriented to biometric recognition. The database size is given in terms of number of generated images; N/A means "not applied" or "not reported".

Method	Biometric Trait	Imaging Task	DB Size
Vascular structure using key points and image texture based on the coefficient of contrast variation [13]	Dorsal hand veins	Synthesis	1,000
Finger vascular structure using a growth method inspired by the generation of venation patterns of plant leaves [4]	Finger vein	Synthesis	50,000
Finger-vein image augmentation based on the data distribution of real images by using GAN networks [19]	Finger vein	Augmentation	N/A
Vascular structure based on anatomy and image translation based on CycleGAN [20]	Finger vein	Synthesis	53,630
Generation of images using a non-parametric texture algorithm [21]	Sclera vessel	Synthesis	N/A
Application of the style-based GAN architecture (StyleGAN) for generating synthetic ROI of palm vein images [17]	Palm vein	Synthesis	60,000
A nature-based method (inspired by the growth of the Physarum polycephalum) for the generation of synthetic ROI of palm vein images [18]	Palm vein	Synthesis	12,000

According to our review, the first work associated with synthetic imaging of vascular structures for biometric recognition appears in [13]. The proposed simulation method starts from randomly but realistically placed nodes¹. Each point in the model is classified as termination, node, or a point belonging to a segment. Once the main points and the number of neighbors are obtained, an intermediate model is explored following some vital rules. After calculating the segments, a dilation algorithm is used to recreate the thickness of the veins. The maximum veins' width is calculated based on the overall dimensions of the simulated hand or entered as a constant. Finally, they recreate the real texture by calculating the coefficient of contrast variation and including some details such as virtual hair. Their findings report that 1,000 generated images are similar to real images but do not provide information on any quantitative or qualitative test results.

In the research proposed by Hillerström *et al.* [4], they developed a methodology to generate synthetic finger-vein images². The proposed model is divided into three parts. First, venous nodes are generated using a growth method inspired by the generation of venation patterns of plant leaves [29]. For this purpose, the procedure takes into account the anatomy of the finger vascular structure, making the distinction of two principal veins on both radial and ulnar sides [22]. The second part is the generation of the vein patterns from the ganglia, connected with a thickened pattern that characterizes the vascular network by dilatation and erosion. The vein thickness is calculated using Murray's law[93], which states that the cube of the diameter of a principal vessel is equal to the sum of the cubes of the diameters of secondary vessels. Finally, the process incorporates the influence of illumination, taking into account parameters associated with the attenuation of transmitted light, optical blur, and scattering. For the paper, the authors generated a

¹The dorsal hand vein simulator is available at <http://veinsim.maditech.ro/>

²The finger vein simulator is available at <https://web.comp.polyu.edu.hk/csajaykr/fvgen.htm>

synthetic database consisting of 5,000 different subjects with 10 synthetic finger-vein images per each, for a total of 50,000 finger-vein images, which is the largest dataset of finger-vein images. To verify the similarity between synthetic images and real images, they use the Bessel K-forms [94] resulting in quite realistic results. Despite this, their database has not yet been used by other studies.

With the rise of Generative Adversarial Networks (GANs), due to their excellent performance for synthetic imaging [95, 96], some authors have adopted GANs architectures to generate finger-vein images [19, 20]. Zhang *et al.* [19] introduced a lightweight GAN architecture to implement finger-vein image augmentation, called FCGAN, which uses a preliminary batch normalization and a tightly-constrained loss function. Their proposal aims to improve Deep Learning methods for finger-vein recognition by reducing training overfitting. Results from experiments on sample augmentation show that CNN converges faster when trained using FCGAN-augmented samples. Hence, it means that FCGAN is able to generate diverse and high-quality finger-vein images, which is useful for improving the training procedure of CNN-based models. Besides, from a visual-quality point of view, the grid effect and the diversity of synthetic samples were analyzed. By using the FCGAN architecture, the strip-shaped creases do not appear in the finger-vein images, generating smoother images. Moreover, FCGAN generates synthetic images with more uneven tones, increasing the diversity of samples. Nevertheless, it should be noted that the proposed approach has only been used for image augmentation rather than creating new samples of different individuals for synthetic database creation.

On the other hand, in [20], they constructed a synthetic dataset of 53,630 finger-vein images corresponding to 5,363 different subjects. For the generation of the images, they first develop the synthetic vein pattern using the algorithm developed in [29] and subsequently perform the translation to images using the CycleGAN architecture [97]. The model learns a correct mapping $X \rightarrow Y$ through a generator, where X contains the data distribution of vascular structure and Y represents the domain containing the image of the structure. Besides, CycleGAN implements a second generator to learn the mutual transformation $Y \rightarrow X$. In order to minimize the difference between the synthetic vascular structure and the real image structure, they use the approach proposed by Johnson *et al.* [98] in the generator. Instead of using a fully-connected neural network as a discriminator, authors used 8×8 PatchGAN [99], which is able to process images of arbitrary size and has a smaller number of parameters. For evaluation, they trained the model with ROI images of the MMCBNU_6000 finger-vein database [100] and validated the synthetic dataset by using five different metrics. Compared against real finger-vein images, experimental results show the generated dataset is very close to the real data distribution, and also venous patterns are better highlighted.

On other biometric domain, Das *et al.* [21] focused on the sclera vessel synthesis to improve the robustness of ocular biometric systems. To produce the synthetic images of the sclera, they develop an algorithm based on non-parametric texture regeneration proposed by [101]. The method consists of modeling the texture as a Markov random field. Thus, given the brightness values of the spatial neighborhood, it is assumed that the brightness probability distribution for a pixel is independent of the rest of the image. Initially, the vein pattern texture is initialized from the source texture with a 3×3 pixel seed. For unfilled pixels, the proposed technique finds a set of patches that most closely resembles the filled neighbors of the unfilled pixel in the source image. One of these patches is randomly chosen, and a color value is assigned to the unfilled pixel from the center of the selected patch. The above process is repeated until the texture is obtained. The experiments were carried out by using the UBIRIS v1 database [102] manually cropped as primitive samples, and they generated a synthetic image for each real one. The proposed experimental setup evidences the usefulness of the generated sclera patterns for biometric purposes. However, it is noteworthy that their implementation is very time-consuming.

Regarding the generation of synthetic palm vein images, it is relevant to highlight our previous conference works presented in [17, 18] and extended in Section 5. These studies preliminary evaluate two generalist techniques that do not explicitly consider the topology of the palm vascular system, but they are pioneers in palm vein imaging. In [17], it is presented a GAN-based approach to simulate the texture of real images. The proposed model was trained with real images from the CASIA database [55] to produce ROI samples of palm vein images. As an alternative, the second work in [18] aimed to reproduce the venous plexus of the palm by establishing an analogy with the patterns formed by the *Physarum polycephalum* [103]. The implementation is based on the algorithm developed in [89] in order to obtain vein patterns. Later, the method fuses the generated vascular pattern with a palmprint image to add details of the palm texture, obtaining a randomly-created sample of palm ROI. By using the proposed approaches, the authors created the largest palm vein databases of the state-of-the-art, as shown in Table 3. Both synthetic datasets were validated through qualitative and quantitative experiments against the most relevant real databases. Taking into account our good previous results in these papers, in Section 5, we formalize a general flowchart for generating synthetic palm vein databases.

Although synthetic databases allow the evaluation of large-scale biometric recognition algorithms, to our knowledge, the vascular pattern images mentioned above have been used little for these purposes. Table 5 summarizes of state-of-the-art approaches applied to biometric recognition using synthetic images of vascular patterns. While synthetic databases allow the evaluation of large-scale biometric recognition algorithms, to the best of our knowledge, synthetic vascular

pattern images have been underutilized for these purposes. Actually, those investigations that cite synthetic databases either use them to improve synthetic databases or as part of state-of-the-art reviews [20, 104]. Focusing on hand veins (back of hand veins, palm veins, and finger veins), probably the low interest in the evaluation of biometric recognition algorithms is because the generation of synthetic vein images has many challenges that prevent an adequate estimation of parameters for their respective simulation. Among the challenges, it is highlighted that the real images present low quality, and the vascular patterns are not observable in the visible spectrum, requiring special devices for their visualization and capture, as shown in Section 2.2.

Table 5: Summary of state-of-the-art approaches using synthetic vascular pattern databases for biometric recognition.

Reference model	Database	Biometric task	Performance results
Hillerström <i>et al.</i> [4], matching binary pattern	Database proposed by the authors	Finger vein verification	EER 1.63%
Yang <i>et al.</i> [20], ResNet34-based model	Database proposed by the authors	Finger vein verification	EER 0.24%
Zhang <i>et al.</i> [19], FCGAN-CNN	Database proposed by the authors	Finger vein recognition and verification	Accuracy 99.67%, EER 0.52%
Das <i>et al.</i> [21], Support Vector Machine (SVMs)	Database proposed by the authors	Sclera pattern recognition and verification	Identification Accuracy 48%, Verification Accuracy 75%
Hernández <i>et al.</i> [105], AlexNet-based model and ResNet32-based model	Synthetic-sPVDB [17]	Palm vein recognition	<ul style="list-style-type: none"> - AlexNet-based model: PolyU 96.00% PUT 93.00% VERA 94.09% - ResNet32-based model: PolyU 99.90% PUT 99.00% VERA 96.82%
	NS-PVDB [18]	Palm vein recognition	<ul style="list-style-type: none"> - AlexNet-based model: PolyU 98.10% PUT 93.00% VERA 94.09% - ResNet32-based model: PolyU 99.30% PUT 98.00% VERA 95.45%

Hillerström *et al.* [4] evaluate the performance of their synthetic finger vein database through an LBP-based model that retrieves and matches local binary patterns from previously enhanced synthetic images, which are obtained by histogram equalization. They then use the Chi-squared distance to calculate the matching scores. Estimate the matching accuracy using 225,000 genuine scores and 1,249,750,000 impostor scores from their synthetic database, achieving an EER of 1.63%. These obtained results suggest the applicability of synthesized finger-vein images for large-scale biometrics applications.

Yang *et al.* [20] propose a model based on ResNet-34 and considers an experimental group and a control group. In the first group, the authors perform a pre-training using their synthetic finger vein dataset, followed by fine-tuning on the MMCBNU_6000 [100] dataset. In the second group, training and testing are performed directly from the MMCBNU_6000 database. The performance verification results in the first group showed an EER of 0.24%, while in the second group, the EER was 0.61%. The above shows that recognition performance can be improved using synthetic images compared to direct training on MMCBNU_6000.

Zhang *et al.* [19] proposed a methodology for finger-vein image augmentation based on GAN networks called FCGAN. For biometric recognition, they a CNN trained with a two-stage progressive augmentation approach. 1) They perform image augmentation with the classical method (using translation in a different direction) and randomly distribute the images equally into ten mutually exclusive groups. Then, each group of finger vein images is fed into the CNN regularly to obtain an optimal result $\mathbb{M}^{(o)}$, as an achieving first-rank classification result. 2) $\mathbb{M}^{(o)}$ is trained sequentially as in the previous stage but using samples augmented with the FCGAN scheme. The authors compare their results with the SAGAN [106] and DCGAN [107] methods of image magnification. The classification accuracy for SAGAN and DCGAN was 98.71% and 98.74%, respectively, while with the FCGAN scheme, they obtained an accuracy of 99.67%. As for the false-positive and true-positive rates, the EER for the SAGAN and DCGAN methods were 0.93% and 0.91%, respectively, while with the FCGAN scheme, they obtained an EER of 0.52%. The above demonstrates that the FCGAN augmentation method can generate higher quality and more diverse finger vein images, which improves the training performance of CNN.

Das *et al.* [21] construct a synthetic database of eye sclera and use support vector machines as the biometric recognition algorithm. Here the authors use five synthetic images of the sclera of the eyes for training and five real images from the UBIRIS database [102] for testing. Estimate the matching accuracy using 10^*5 for false rejection rate (FRR) and 10^*9^*5 scores for false acceptance rate (FAR), thus achieving an accuracy of 48% for identification and 75% for verification. From the results obtained in this research, the synthetic image generation method was not adequate.

Finally, Hernández *et al.* [105] evaluated two end-to-end CNN architectures (based on AlexNet and ResNet32) on the Synthetic-sPVDB [17] and NS-PVDB [18] datasets for biometric recognition. Both models were trained on the two synthetic databases and validated by a cross-testing scheme on the most representative real databases of the state-of-the-art. Experimental results are higher than 93% for the AlexNet-based model trained on both synthetic datasets. In the case of the ResNet32-based model, reported results are comparable with those reported in the literature on the public databases.

Although using synthetic vein pattern databases in evaluating biometric recognition algorithms is still limited, state-of-the-art results described above show the feasibility of their use in vascular-based biometrics.

4.2 Generation of Vein Patterns Related to Biological Networks

The formation of venous structures with a perspective oriented to biological transport is relevant in the biometric context because they reproduce patterns and predict measurable quantities. Biological transport networks are part of the critical infrastructure required to distribute resources quickly and efficiently throughout the body. They include the vascular systems of plants, animals, plasmodial veins of slime molds, among others. Vascular networks play a key role in the overall organization of the body. Furthermore, there is evidence that vessel size and network architecture follow fourth power allometric scaling laws that relate the fractal branching pattern of the network to body size and metabolic rate according to metabolic scaling theory (MST) [108], or reflect the design of optimal transport networks [109, 110, 111].

A venous network is composed of tubular elements with different thicknesses and lengths organized as a hierarchical branching tree. The structure obtained can be open or closed, with a significant number of additional loops to improve performance under fluctuating loads or in the presence of damage [112, 113]. Blood vessels have geometric characteristics that impact local blood flow, although their general flow behavior and scale relationships exhibit other networks' properties.

There are a wide variety of models that allow the representation of open and closed vascular structures. This section presents an updated review of models, and we have classified them into three categories: (i) solving dynamical systems, (ii) computational modeling, and (iii) geometrical methods. In Figure 7, the models have been classified according to these categories and taking into account the parameters associated with the models, which can be phenomenological, qualitative, or hybrid (combination of models). These models can be considered part of a constructive theory, which maintains that every system is destined to remain imperfect. However, nature distributes them optimally from the global optimization of local constraints [114].

The networks generated by the numerical resolution of dynamical systems are based on the assumption that the network evolution can be represented by partial differential equations that model the growth phenomenology [27]. Computational modeling consists of producing discrete events through a series of dynamic attributes (phenomenological or qualitative) defined locally on a dataset; this allows the network to evolve over time with a minimum of a priori assumptions [29]. Likewise, we have classified the models considering their applications and parameters in Table 6.

Among the models for solving dynamic systems to generate vascular structures are those based on reaction-diffusion methods [115]. These models produce theoretical open and closed vascular structures from phenomenological principles with realistic parameter values [139]. Based on this approach, vascular networks are the result of two mechanisms: (i) vasculogenesis, which is the formation of new blood vessels from a population of endothelial cells, and (ii) angiogenesis, which is the formation of new blood vessels from pre-existing vessels. In the case of vasculogenesis, it is assumed that the mechanism driving vascular network formation is due to cell traction forces that provide local chemical signals that attract cells to initiate venous patterning [140].

Applying reaction-diffusion models present some weakness. The vasculature contains a range of spatial scales, which cannot be controlled respecting allometric scale laws [108]. In addition, a highly interconnected network is assumed that vessel pressures at nearby spatial locations are correlated [141]. We emphasize that modeling through dynamical systems allows the generation of closed structures. Therefore, there is a particular interest in this type of model producing vascular networks assuming anisotropic structures such as those formed in the skin [142]. The method assumes that external chemicals in the environment attract/repel and exert drift forces that direct the formation of

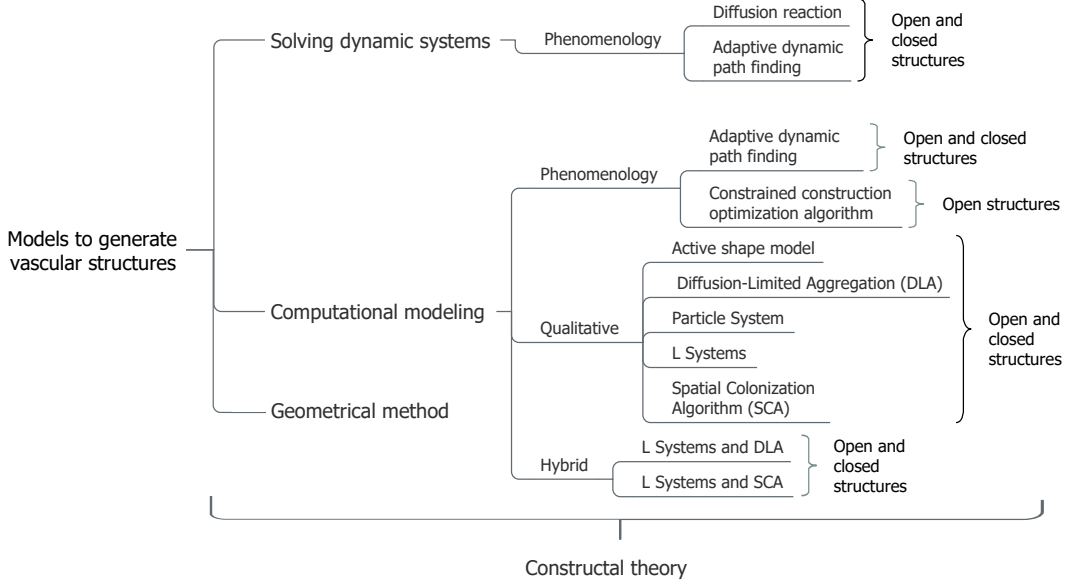


Figure 7: Classification of models used in the generation of biological vascular structures.

Table 6: Summary of the state-of-the-art models for the generation of biological vascular structures.

Model	Type	Parameters	Application
Reaction-diffusion systems [115]	Solving dynamic systems	Diffusion rates and reaction parameters (nonlinear functions)	Cell growth [115], plants venation [116], and wing vein patterns [117]
Adaptive dynamic pathfinding [118, 119]	Solving dynamic systems and computational modeling	Concentration and nutrient gradients	Pattern generation formed by the foraging of some multicellular organisms (i.e. <i>Physarum polycephalum</i>) [118, 119]
Constrained constructive optimisation [120]	Computational modeling	Intravascular volume and branching angles (cost function)	Complex arterial trees [121, 122], human cerebrovasculature [123]
Active shape model [124]	Computational modeling	Reference points of real images	Retinal vascular network [125]
Diffusion-limited aggregation [126]	Computational modeling	Density correlations in terms of the distance separating the two sites	Branching structures (arteries/veins) [127], river networks [128], simulation of natural texture [129]
Particle system [130]	Computational modeling	Particle distribution and motion	Leaf structures [130] and topology optimization of heat conduction systems [131]
Lindenmayer system (L-system) [132]	Computational modeling	Branching angles, elongation rates and vigor of branches	Virtual plants [132], retinal vasculature [26] and blood vessel [133]
Space colonization algorithm [30]	Computational modeling	Attraction points, radius of influence and kill distance	Branching structure of trees [30], leaf venation [29], finger vein images [4] and tracheal gills of mayfly larvae [134]
Hybrid models [135, 136]	Computational modeling	Parameters associated with the models: L-system–Diffusion-limited aggregation and L-system–Space colonization algorithm	Leaf venation patterns [135] and complex structures [136].
B-spline based vascular structures [137, 138]	Geometrical method	Control points or vector of nodes	Flexible vascular representation [137], Retinal vascular network [138]

vascular networks to specific sites. The general model is defined by the system of partial differential equations as follows,

$$\begin{aligned} \partial_t \eta &= -\nabla \cdot (\eta \mathbf{v}) \\ \partial_t \mathbf{v} &= \mathbf{v} \cdot \nabla \mathbf{v} + \beta \cdot \nabla \mathbf{c} - \gamma \mathbf{v} - \nabla \psi(\eta) \\ \partial_t \mathbf{c} &= \mathbf{D} \Delta \mathbf{c} + f(\mathbf{c}, \eta) \end{aligned} \quad \left. \right\} \quad (1)$$

where η is the endothelial cell population, \mathbf{v} defines the flow direction, β is the intensity of the cellular response, γ is the drag factor with respect to the substrate, $\nabla \psi(\eta)$ measures the response of the set of cells to deformations, \mathbf{c} is the

vector of chemoattractants-chemorepellants, \mathbf{D} is a diagonal matrix containing the diffusion coefficients, and $f(\mathbf{c}, \eta)$ is the function that induces the reaction between η and \mathbf{c} .

As part of reaction-diffusion systems, Meinhardt [143] introduced a new model based on activator-inhibitor and activator-substrate chemical gradients to generate network-shaped structures that allow the water supply, oxygen, and information on a tissue. The orientation results from local signals that spread as the network grows, and the cells respond by differentiating into members of the branch system. Differentiated cells are supposed to eliminate growth signal-generating tropic substances, making the system sensitive to minute differences in concentration. The formation of branches occurs in two ways: lateral branching if new growth signals are activated along the branches, or a dichotomous branching if the growth signal is divided at the ends of the branches. Among the applications that have been given to the model are the generation of blood networks, insect tracheas, axons, or leaf veins [116, 143, 144].

Moreover, the systems based on activator-inhibitor and activator-substrate principles have shown how interactions at the molecular level can lead to morphogenesis and differentiation for angiogenesis. Dorraki *et al.* [145] review the dynamics of angiogenesis to study tumor growth, where they show models of continuous focus with other parameters such as components of the extracellular matrix, oxygen, migration, and proliferation of endothelial cells. The models considered in [145] although describing the dynamics better, are not intended to generate branched structures.

Pathfinder-based models with adaptive dynamics are representative of both resolution of dynamical systems and computational modeling (see Figure 7). For generating a network, the parameters used are characteristic of phenomenology and allow the construction of open and closed structures. Such models are inspired by the conduct of organisms whose survival depends on optimally seeking pathways to nutrient sources. These kinds of adaptive dynamics have also become used in the construction of heuristic algorithms in optimization processes [146, 147]. In this sense, an algorithm based on *Physarum polycephalum* has allowed the creation of vein networks similar to those found in living beings [118, 119].

The growth of *Physarum* has been modeled through the resolution of dynamical systems assuming Jean-Baptiste Lamarck's first law, which establishes the development of animal organs based on their utility [148]. Lamarck's first law could be interpreted as the vessels' diameters increasing depending on the flow rate [149]. The network begins with sources and sinks located in an arbitrary mesh generated by a Delaunay triangulation. The tubular thickness adaptation is a function of the conductivity at the node (i, j) that changes in time according to the expression

$$\frac{dD_{ij}}{dt} = f(|Q_{ij}|) - D_{ij} \quad (2)$$

where D_{ij} is the fluid conductivity and f is a continuous monotonic increasing function that depends on the flow rate Q_{ij} and satisfies $f(0) = 0$. In addition, f represents a coarsening factor that increases with the flow, and $-D_{ij}$ is a thinning factor. The coarsening component dominates for a channel with a larger flow, and the thinning effect dominates for small flows at each time step. The complete time evolution of the network is calculated iteratively with the updated conductivities.

On the other hand, computational modeling of pathfinding with adaptive dynamics employs an agent-based layer and a path layer that affect each other. Thus, agents deposit a trace on the path map, while those particles detect values from the map to determine aspects of their movement [119]. Each agent has a heading angle, a location, and three sensors (front left, front, front right). The sensor readings affect the particle's heading, causing it to turn left, turn right, or stay in the same direction. The paths undergo a diffusion and decay process at each time step.

Also within the computational modeling context are constrained constructive optimization algorithms, which use parameters that depend on phenomenological features and allow the generation of open structures. This approach produces complex dichotomously branched arterial tree models that have been shown to reproduce key structural features of coronary arterial trees [150]. Network generation is sequential and driven by the constrained minimization of a cost function designed to minimize the energy expenditure of blood supply to surrounding tissues [122]. The construction of a model tree is achieved by the stepwise addition of individual segments that simulates natural growth. At each step, this growth is guided by an optimization objective and by ensuring the growing tree meets geometric conditions between vessel diameters at a bifurcation following Murray's law, as well as a specific pressure or flow at the tree terminations [151]. A set of pseudorandom numbers is used to determine the sites of new segments, which become the main branches of the fully developed tree in the early stages of development. Therefore, the topography of these main branches is highly dependent on the set of pseudorandom numbers used [120].

Constructive constrained optimization algorithms address different types of studies involving the influence of anatomical variability, bifurcation asymmetries, fractal properties, and stepwise growth [122]. Also, some variants have been proposed to recreate more complex vascular networks in hollow organs or to accelerate the construction of such networks using heuristic optimization algorithms [123]. Particularly, Bui *et al.* [121] used a constrained construction

optimization algorithm to produce cerebral vasculature with a preferential distribution of large arteries in the cerebral cortex. Besides, Georg *et al.* [152] simulate a hepatic venous tree generated in stages following fractal behavior.

An alternative way to produce vein networks is using active shape models, which are part of computational modeling and provide a statistical representation of shapes from real image landmarks, allowing both open and closed vascular structures to be generated [124]. Training samples are aligned in a common coordinate frame, and deviations from the mean shape are analyzed. Each training shape is represented as a fixed number of n landmarks placed along an equally spaced grid. These reference points form a vector, which is subsequently reduced by principal component analysis (PCA), assuming that the most relevant features are those with the highest variance. Such models allow a variety of structures to be generated since they use reference images. Particularly, in [125] they use an active shape model to generate synthetic images of the retina. The disadvantage of the method is that good-quality images are required for segmenting the vascular networks to reproduce the desired structure. While allowing the generation of vascular structures, the previous model is not explicitly focused on this but rather on reproducing variations of any shape. In contrast to this approach, the following will describe computational models specifically focused on vascular structures.

Diffusion limited by aggregation (DLA) is a process attributed to Forrest and Written [126]. This process involves subjecting a set of particles to a random walk so that they subsequently agglomerate around a particle called the seed. The DLA starts with the seed at a fixed position within a bounded region. The particles are then randomly released from the edge and follow a Brownian motion until reaching the seed; highly branched or solid structures can be achieved by introducing a sticking probability [127, 153]. Other variants of this approach have also emerged, such as Cluster-Cluster Aggregation [154], which starts with a system of particles that diffuse in space and form clusters when they meet. These, in turn, can interact with other clusters or particles to form even larger aggregates. In [129], the authors propose the Random Drop Ballistic Aggregation algorithm. Instead of using a Brownian motion to form the aggregate, they define a radius and direction on the particles to choose the closest adhesive position of the cluster. Their method uses a kernel that can change the adhesion conditions, limiting the growth according to the clusters and inhibiting the formation of long tendrils.

As in the continuous models, the disadvantage of the DLA algorithm is that it is not possible to control the allometric scales. Despite this, network growth by DLA tends to occur at the extremes of the structure, and particles are less likely to reach the inner parts. This feature operates across scales and gives rise to a fractal nature, which can be associated with physical and chemical properties. This model is used to simulate growth patterns that appear in some organic and non-organic phenomena such as crystal growth, the trajectory described by lightning, vascular systems, among others [127]. Particularly, in [128] show that the structures of river and leaf vein networks are statistically similar and can be simulated on a small scale using aggregation-limited diffusion.

Lindenmayer systems or L-systems allow studying various aspects of vascular pattern formation following a fractal behavior [132]. The branching information and changes in topology are realized using a mathematical construct called a rewrite or production rule. A rule is written as predecessor-successor; the successor in the resulting string iteratively replaces the predecessor. On the other hand, to account for external factors such as length and angle dimensions that may vary at each rewrite step, a perimetric L-system is defined [132]. Among the applications of L-systems are the generation of 3D synthetic blood vessels by adding stochastic parameters [133] and the generation of retinal venous structures, which is relevant in diagnosing and treating diseases affecting the eyes. The retinal vasculature is realized by an inverse L-system problem, in which the rules must be obtained from images representing the tree-like structure [26].

The particle system is an algorithm for generating leaf vein patterns for realistic synthetic images [130]. This algorithm initially distributes a set of particles over a leaf-shaped region. The particles move towards a sink located at the base. In the process of displacement, they attract each other and merge when they reach a distance threshold. The venation pattern is the result of the trajectories taken by the particles. Some of the patterns generated develop primary and secondary veins that are typical of open venation structures. This algorithm has also been used in the topological optimization of structures for heat conduction [131].

The spatial colonization algorithm is a model for generating highly irregular leaf venation patterns [29]. The model works by iteratively extending the partially formed veins to points considered sources of a vein-inducing signal. Sources are dynamically added as the leaf grows and removed as veins approach them. Also, the algorithm generates morphological properties, such as each branch's length, diameter, and angles, through Murray's law. The branching structures have a hierarchical order, with the first-order veins being the largest in diameter. Higher-order veins may have a free end, producing an open veins pattern or anastomose, forming loops characteristic of a closed pattern. The parameters taken into account in the algorithm are the attraction distance, the elimination distance, and the length of the segments. The spatial colonization algorithm has also allowed the generation of other types of structures. In [4], they use the algorithm for the generation of synthetic images of finger veins, and in [134] simulate the branching patterns of mayfly gills to investigate the global mechanism driving their generation and morphological evolution.

The hybrid models combine two or more models to improve both the performance and the quality of the vein network structure. In [135] they propose a method that combines spatial optimization algorithm with L-systems to accelerate the growth of the leaf vein network. Their results show that the properties of the network can be improved in a minimum time. In [136] combine L-systems with DLA to model novel growth structures. Particularly, L-systems are used to guide DLA simulations [136].

Finally, B-spline-based mathematical models are segmental interpolators generating smooth curves and using control points to form realistic vascular structures [137, 138]. The control points are defined at main points in the network, such as bifurcations or terminal points. Different B-spline types have been used for the elaboration of vascular networks. In [137], the authors use non-uniform rational B-spline (NURBS) to reproduce vascular network models based on physiological or image-based parameters. NURBS allows to adjustment of the shape of a curve through a weight parameter. On the other hand, in [138] introduce the Catmull Rom spline (a particular case of NURBS, when the weight parameter is equal to zero) to simulate the Retinal vascular network, determining the control points from the temporal arcade. Although B-spline allows the generation of realistic vascular networks, it is not a model for generating vein networks. Instead, it is a technique that allows efficient point along with the characteristic that the resulting curve is differentiable at all points, thus providing images with a high degree of realism.

5 Evaluation of General-Purpose Approaches for Generating Synthetic Palm Vein Images

In the following, we present and evaluate two different approaches for the generation of synthetic palm vein images, which were firstly introduced in our conference papers [17, 18]. Based on our previous results and the review of the state-of-the-art, we formalize a general flowchart for the creation of a synthetic database, as shown in Figure 8. The proposed methods are focused on generating region-of-interest (ROI) samples of palm vein images since usually SOTA methods for palm vein recognition use the ROI from a human hand.

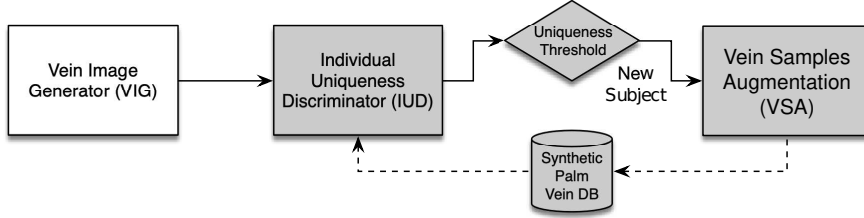


Figure 8: Overview of the flowchart of studied approaches for generating synthetic palm vein images and creating a synthetic database. The processes highlighted in gray color are common to both approaches, whereas the VIG process varies depending on the generation method implemented.

The purpose of this section is not to provide a large-scale database of palm vein images per se, and in any case, do not replace datasets of real-world images. Thus, it aims to explore options from the state-of-the-art to generate palm vein samples, both computational and mathematical methods. Hence, the created synthetic datasets can be alternatives to quickly estimate the efficiency, scalability, and general performance of newly or formerly designed approaches for palm vein recognition on a larger dataset than the currently publicly available ones.

The proposed flowchart comprises three main procedures; whereas the first one varies depending on the generation method implemented, the last two processes are common to both approaches. Each process is described as follows:

- 1. Vein Image Generator (VIG):** The VIG procedure aims to generate random synthetic images that simulate both the vein patterns (i.e. dark gray patterns of vascular structures) as well as visual characteristics (i.e. texture, contrast, and illumination) of palm vein images. As was analyzed in Section 4, it is important to notice that there are different methods to produce synthetic vascular structures. Thus, the presented model can be implemented using a variety of approaches by modifying the generator in correspondence with the other parameters involved in acquiring real images of palm vein patterns. Therefore, we evaluate two different general-purpose methods to implement the VIG procedure. We firstly analyze a novel specific domain application for the style-based GAN architecture (StyleGAN) [88] for generating synthetic palm vein images, which is presented in Section 5.1. Under the foundation that the acquisition process produces images with very particular characteristics in terms of texture, illumination, and contrast, this approach aims to generate synthetic palm vein images of unique individuals, simulating the same style of the real images. Later, in Section 5.2, we examine a nature-based approach for simulating the palm vein plexus, which is inspired in the

natural transport network by the growth of the *Physarum polycephalum* that forms path patterns similar to vascular structures.

2. **Individual Uniqueness Discriminator (IUD):** The previous procedure randomly generates synthetic palm vein images, satisfying the uniqueness requirement to be part of a biometric database. Therefore, the IUD procedure compares each newly produced image against all samples in the synthetic database to ensure the uniqueness requirement. Since the process of creating the synthetic database is incremental, we adopt a matching procedure based on a uniqueness threshold by computing the similarity score proposed in [91]. In accordance with the experiments of [91], we fix the uniqueness threshold to 0.1 as a good separability criterion of genuine and impostor samples. Hence, the generated image is discarded if the computed similarity score with any instance in the database is higher than the uniqueness threshold. Otherwise, if the threshold is not exceeded for any of the samples in the database, the generated image satisfies the uniqueness criteria and is incorporated into the database as a new subject. Because an exhaustive search must perform the similarity matching process in the database, we implemented a multi-thread algorithm [91] to reduce processing time.
3. **Vein Samples Augmentation (VSA):** Since a biometric database should contain more than one sample per individual (e.g. gallery and probe samples), in order to increase the number of samples per subject, we perform a sample augmentation process for each new unique image generated by the IUD procedure. Thus, the VSA procedure aims to obtain different samples for each subject by applying random transformations on the image to simulate natural variations of a real-world contactless acquisition process of palm vein images. For this purpose, two kinds of transformations are randomly applied over the primary sample: texture/illumination variations (i.e. contrast, lighting, and blurring), to simulate the effect of NIR illumination, and affine transformations of the ROI (i.e. translation, rotation, cropping, and shear), to replicate changes of the hand position on the acquisition device. Finally, we obtain six samples per each new subject in the database.

5.1 Generation of Style-based Synthetic Palm Vein Images

As mentioned in Section 4.1, different approaches have adopted GAN variants for sample augmentation purposes in finger-vein recognition. Besides, GAN-based methods have been proposed for generating iris [155, 156] and face images [157, 158]. Thus, taking into account their previous proposals, we study the effectiveness of the StyleGAN architecture [88] to implement the VIG procedure, aiming to simulate the visual characteristics of palm vein images in terms of texture, illumination, and contrast. Among GAN variants, the StyleGAN2 model [159] has demonstrated to achieve better results in terms of image quality, images variability, and efficiency, improving the former architecture and generating more realistic images. Hence, we firstly implemented a StyleGAN-based vein image generator (Style-VIG) aiming to create random palm vein samples and reproduce the *style* of real palm vein images with a high level of realism.

Figure 9 depicts the GAN-based approach implemented by the Style-VIG process. Firstly, the StyleGAN model transforms the Input Latent Code (z) by mapping it into an Intermediate Latent Code (w), which encodes the style of the real images. Thus, the Generator (G) synthesizes new samples from the mapped coded (w) by adding random noise to facilitate the stochastic variation. The StyleGAN2 architecture improves the original StyleGAN model by applying the bias and noise operations on normalized data used in the generator, which helps to remove normalization artifacts from generated images. On the other hand, the Discriminator (D) learns to distinguish real and fake images by training a binary classifier from real training images. Thereby, both networks are trained collaboratively meanwhile fine-tuning each other by minimizing the GAN loss function.

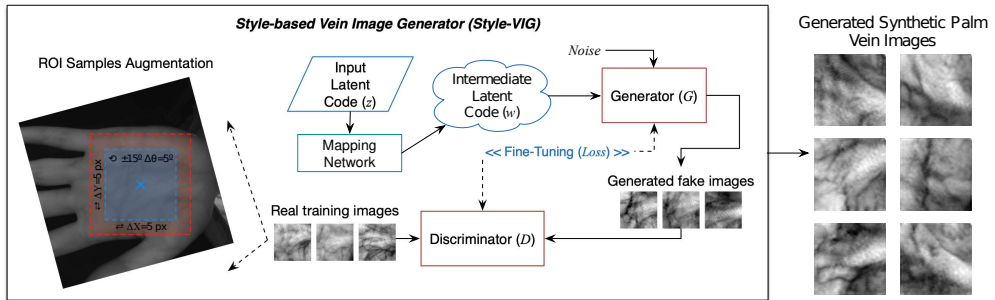


Figure 9: General scheme of the StyleGAN-based Vein Image Generator (Style-VIG), which is based on the StyleGAN2 model.

Due to public datasets of real images have a limited number of samples, a challenge to face is the lacking of training data. Hence, different from other approaches that apply image augmentation from the ROI samples during the training process, we implemented a ROI sample augmentation procedure during the pre-processing stage. Thus, we obtain 87x ROI samples from each raw image by translating and rotating a central ROI (blue square) within the entire palm (red square). The central ROI is centered on the palm region, which its side is determined by the middle points between the index and middle finger, and the ring and little finger, respectively. To augment the number of ROI samples, the central ROI is repeatedly shifted in both axis with $\Delta(X, Y) = 5px$, and also it is rotated by $\Delta\theta = 5^\circ$ up to $\pm 15^\circ$, both clockwise and counter-clockwise.

In our experiments, we trained the StyleGAN2 network [159] on the 850nm-band of CASIA dataset [55], which is commonly used for palm vein recognition. Hence, the training data was originally comprised of 1,200 real images, which were increased up to 104,400 training samples after performing the procedure for ROI samples augmentation. Our implementation was based on the official StyleGAN2 source-code from NVIDIA Research Projects³. We used the original configuration (config-e) of the architecture to train the StyleGAN2 model for 25,000 k-images. Finally, the training process reported a Frechet Inception Distance (FID) equal to 63.89. Whereas the training process took five days, the generation process takes on average 58.1ms (± 259.69 ms) to create a new synthetic sample.

Besides, as part of the present work, we extended the Synthetic-sPVDB dataset [17], reaching a total of 20,000 individuals and 120,000 synthetic samples. This second version has been possible thanks to the incremental generation process aiming to increase the number of individuals in the database. As is noticeable in Table 3, compared to the largest real database Tongji [58], the proposed dataset is the largest of the state-of-the-art, being 33 and 10 times larger in the number of subjects and the total samples, respectively.

5.2 Generation of Nature-based Synthetic Palm Vein Images

As the second approach for implementing the VIG procedure, we developed a slightly more specific method based on biological transport networks. In this case, we aimed to examine a mathematical model for simulating the palm vein plexus and comparing the previous general-purpose computational model against a natural-inspired one. The idea behind this method is based on the principle that the vascular network adapts its structure in an optimal way to the hand's movement and muscles. Thus, we implemented a mathematical model based on pathfinding with adaptive dynamics, which have been used to simulate the growth of the *Physarum polycephalum* [103]. Particularly, the *Physarum polycephalum* dynamically forms regular path patterns similar to the vein plexus network since its growth patterns establish optimal organizational structures with high efficiency.

In the literature, there are different mathematical approaches for modeling the growth of the *Physarum* [160, 161, 89]. Particularly in [89], the authors propose a multi-agent model to simulate the growth of the network structure. The proposed model uses a simple process to produce the complex patterns of the *Physarum*, which is based on two requirements: optimal searching of nutrients within the maximum area and the loop formation to ensure a fault-tolerant transport network. Thus, since palm vein patterns should satisfy similar optimization processes to supply blood to the entire surface of the hand, we used the mathematical model of [89] to simulate an approximate structure of the palm vein patterns. An overview of the proposed nature-based VIG process is shown in Figure 10, which is called Nature-VIG and is comprised of three sub-processes described following.

Firstly, the *Physarum* Generator is used to generate a vascular network by using the multi-agent model proposed in [89]. The multi-agent model is based on a self-organized system approach, which uses two types of agents and three transition rules to simulate the network's behaviors and interaction, respectively. The growth of *Physarum* is characterized by adaptive search and contraction behaviors considering global and local conditions of the environment. Initially, the agents randomly move within the square representing the palm ROI and then converge to the most optimal network to connect the food sources located in the midpoints of the top and bottom of the region, which analogously correspond to the proximal to the distal part of the palm. This random search process is performed iteratively, where the higher the number of iterations, the more different types of patterns are formed due to the contraction behavior. According to the experiments performed in [89], for more than 200 iterations, the dynamic change of the agents tend to converge to a steady pattern by reducing the number of loops. Hence, in our model, we set this parameter by a random number from 350 to 700 iterations, which, jointly with the initial random movement of the agents, ensure the inter-class variations of the generated samples.

The second sub-process of the Nature-VIG procedure aims to enhance the vascular patterns produced by the *Physarum* Generator. We apply both brightness and blurring filters over the vascular image to reduce the discontinuities formed by the agents' imprint obtaining a continuous vascular structure and simulating the NIR illumination effects occurring in the acquisition of real images, respectively. Thus, the brightness variations are randomly applied, increasing the overall

³<https://github.com/NVlabs/stylegan2>

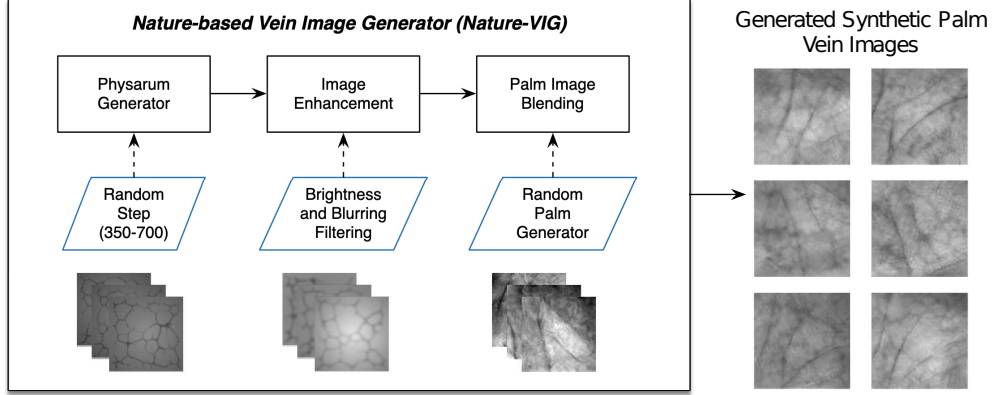


Figure 10: General scheme of the Nature-based Vein Image Generator (Nature-VIG), which is based on the growth of the *Physarum polycephalum*.

illumination between 1.2 and 1.8 as a factor of the original brightness. Afterward, we compute a sequence of extended box blurring filters over the obtained images, which uses a Gaussian kernel (with $radius = 3 \sim 5$) [162].

Finally, to obtain the final palm vein image, we blend the previous enhanced image with a randomly generated palmprint image in order to add palmprint details and texture. For this purpose, we trained a StyleGAN2 model [159] to randomly generate palmprint images based on the images of the CASIA database [55]. For training the GAN model, we used ROI samples from the visible spectrum (WHT) of CASIA because they were collected with the same acquisition protocol of palm vein images in the dataset. Thus, to augment the number of training samples, we employ the same image augmentation process described for the Style-VIG process (Section 5.1), obtaining 104,400 samples from 1,200 palmprint original samples. As well as for the Style-VIG process, our implementation of the StyleGAN2 model was based on the NVIDIA Labs' implementation. The model was trained for 25,000 k-images with a final FID equal to 77.28. Lastly, after having executed all the sub-processes of the Nature-VIG procedure, we get the final image of synthetic palm vein patterns on average time up to 179.32 (± 37.29) seconds.

As for the previous generation method, we have increased the size of the NS-PVDB database obtained by the Nature-VIG procedure. Thus, we generated 96,000 synthetic samples corresponding to 16,000 different subjects. Since the nature-based simulation of vein patterns is more time-consuming than the GAN-based approach, it has not been possible to achieve the same size as for Synthetic-sPVDB; however, we will continue to increase the dataset's size.

5.3 Performance Analysis of Generated Synthetic Images

In [17] and [18], we performed both qualitative and quantitative evaluations to compare the similarity between real and synthetic datasets. For the qualitative assessment, we used the Gray-Level Co-occurrence Matrix (GLCM) [163], the Deep Image Structure and Texture Similarity (DISTS) index [164], and the Structural Similarity Index (SSIM) [165]. Also, we compute quantitative metrics such as the Frechet Inception Distance (FID) [166], the Accuracy of a binary classifier to predict real and generated samples, and the $F_{1/8}$ and F_8 metrics proposed in [167]. In the evaluation, we compared the generated datasets against the most relevant public databases. The experimental results suggested that synthetic and real palm vein samples share visual features verifying the realistic characteristics of the generated datasets.

The following sections present an extension of the previous validation of the proposed synthetic datasets [17, 18]. We carry out new experiments aiming to deepen our understanding of the similarity between real and synthetic palm vein samples. First, we conduct a human inspection of random samples from the public database and the generated datasets to understand the visual perception for classifying both sets of images. Second, we analytically model the lower-order similarity of textures by using Bessel K forms [168, 169]. Finally, the evaluated quantitative metrics are computed on the databases not considered in the conference papers [17, 18].

The experiments were performed on a dedicated server comprised of two Intel Xeon Gold 6140 CPUs (36 physical cores), 126GB of RAM, and four NVIDIA GeForce GTX 1080Ti GPUs. The models were implemented using Python 3.7 and OpenCV 4.1, while the implementation of StyleGAN required TensorFlow 1.15, CUDA 10.1 toolkit, and cuDNN 7.5. Additionally, the created synthetic datasets are available online at: <http://www.litpr.cl/repository.html>.

5.3.1 Visual Evaluation by Human Inspection

Intending to examine the human perception of palm vein images produced by both generation methods studied, we developed a human inspection experiment to classify ROI images of palm veins into real or synthetic. For this purpose, we invited 40 people separated into two groups according to their experience related to image processing and vascular biometrics. Thus, the first group was integrated by 20 researchers in the mentioned areas from countries such as Chile, Argentina, Colombia, and Spain. On the other hand, the second group was ordinary people with no experience or knowledge in the research area. Therefore, the group of researchers allowed us to establish a control group for other participants' responses.

To carry out the experiment, we created an online application to show palm vein samples to the participants and ask them to choose which from a gallery were real images. Initially, as depicted in Figure 11(a), the application showed a first screen displaying random samples from publicly available databases, where participants could familiarize themselves with the visual characteristics of this type of image. Later, a gallery of 12 random images was shown like in Figure 11(b), 6 of which correspond to real samples from public datasets, and the other 6 were from our synthetic databases. Then, each contestant had to choose six samples that he/she considered to be real.

Figure 11(c) shows a bar chart plotting the percentage of each type of sample that was classified as real by each participant. In the graph, numbers from 1 to 20 correspond to the control group of researchers, whereas from 21 to 40 are ordinary contestants, and the last bar is the responses' overall average. Table 7 also summarizes the average percentages of each group. From the results, it is supposed that the higher the percentage of synthetic samples classified as real, the greater the similarity of these images.

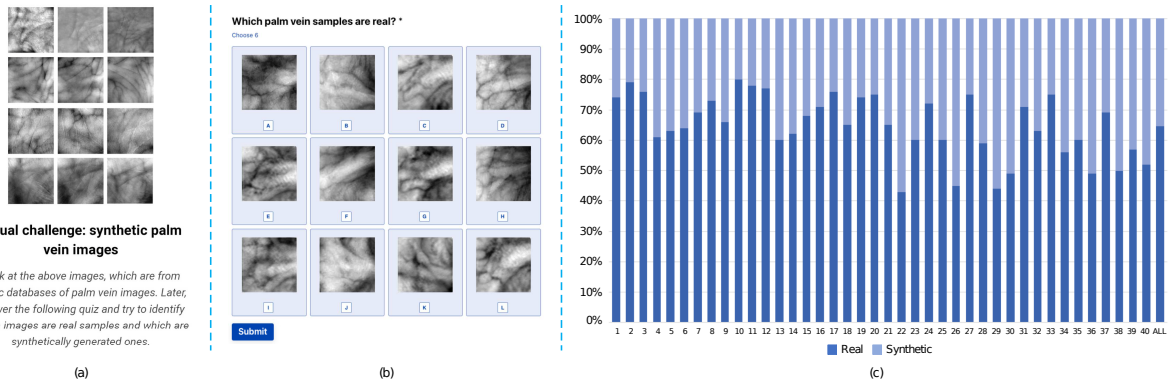


Figure 11: Examples of the visual inspection application (a)(b) and the corresponding bar chart from the participants' responses (c).

Table 7: Average classification percentages of each group in the visual evaluation.

Group	Real Samples	Synthetic Samples
Researcher	70.55	29.45
Ordinary	58.70	41.30
All	64.63	35.37

It can be noticed that although on average more than 40% of the synthetic samples were classified as real by the ordinary group, this value was about 11% lower for the control group. On the one hand, this behavior was partly influenced by the fact that the images were randomly displayed from the databases. Besides, according to previous qualitative and quantitative tests [17, 18], the generated databases have more similarity to some of these. In order to compare palm vein patterns from different public databases and the generated synthetic datasets, Figure 12 shows ROI samples and the vein patterns extracted from them. It is possible to appreciate the existing visual similarities in the original and segmented images using skeletonization and binarization of the vein patterns, respectively. In addition, similar cyclic structures corresponding to the venous network of the hand are observed in the vein patterns obtained. Although the two types of images have certain visual similarities, it is worth noting that unrealistic details can be presented in some cases. Consequently, a small grid effect can be observed for the images produced by the Style-VIG generator. In contrast, non-homogeneous textures of vein patterns are produced in the samples generated by the Nature-VIG procedure.

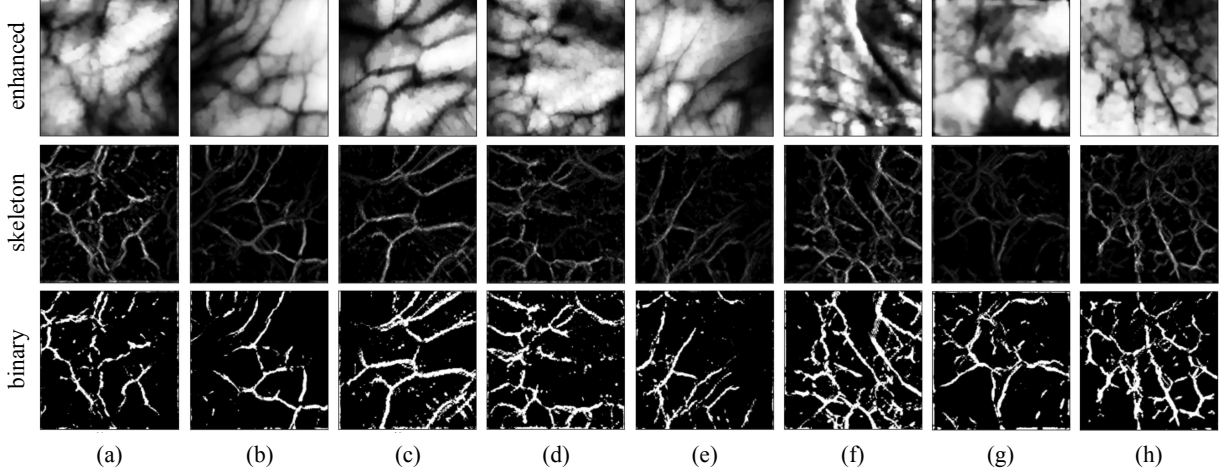


Figure 12: ROI samples and the extracted vein patterns from different public datasets: (a) CASIA, (b) PUT, (c) PolyU, (d) Tongji, (e) IITI, (f) FYO, (g) Synthetic-sPVDB, and (h) NS-PVDB. The first row shows enhanced ROI images, while the second and third rows contain the skeletonization and binarization of vein patterns, respectively.

5.3.2 Similarity Analysis based on Probability Densities of Pixels Distribution

In the literature, different works in the area of synthetic biometric imaging [16, 4] use the Bessel K-forms [168] as a method to compare the lower-order similarity of images textures. Thus, this section establishes a texture-level distinction between real and synthetic samples following the same methodology. The method models the lower-order probability densities of bandpass filtered images and allows comparison of the studied images [16]. The Bessel k-forms is a parametric family that depends on two parameters: shape p and scale c , as shown in Equation 3:

$$f(x; p, c) = \frac{1}{Z(p, c)} |x|^{p-0.5} K_{p-0.5} \left(\sqrt{\frac{2}{c}} |x| \right), \quad (3)$$

where, $K_{(p-0.5)}(\sqrt{2/c}|x|)$ denotes modified Bessel functions of the second kind and Z is the normalizing constant given by $Z(p, c) = \sqrt{\pi} \Gamma(p)(2c)^{0.5p+0.25}$ [168].

It is worth mentioning that each filter selects and isolates certain features present in the original image, and they depend on the specific task. For K-form modeling, in [169] suggest filters whose resulting spectral components have marginals with the following characteristics: 1) unimodal with the mode at zero, 2) symmetric around zero, and 3) leptokurtic. Particularly, in this analysis, we use the log-Gabor filter, as well as in [4]. The estimation of the parameters p and c for the K-forms can be determined from the observed data by the expressions:

$$\hat{p} = \frac{3}{SK(I) - 3} \quad \text{and} \quad \hat{c} = \frac{SV(I)}{\hat{p}}, \quad (4)$$

where, SK and SV are the sample kurtosis and variance of the filtered image I , respectively.

To compare real and generated palm vein images, we use the Bessel K-shape representation, as it allows us to quantify the degree of disorder of the veins. For the initial comparative analysis, we randomly selected ten samples from five different datasets: synthetic palm vein samples from the Synthetic-sPVDB and NS-PVDB databases, real images from the PUT [64] and CASIA [55] datasets, and natural images from the Imagenet database [170]. The images were scaled to the same size, and the intensities of gray levels were normalized, and then the log-Gabor filter was applied. Figure 13 comparatively show examples of each set of images with their corresponding filtered image and the associated curves with the observed and estimated pixel densities with the Bessel K-forms.

Table 8 presents the values of the parameters of Bessel K-forms estimated from the filtered images. It can be seen that the shape parameter p oscillates in a wide range from a synthetic image to a real image, but this same behavior can be observed in the CASIA database, whose values range from 0.38 to 2.38. This behavior is reasonable since the palm vein patterns do not have a particular shape, and also, the images are influenced by many parameters as explained in

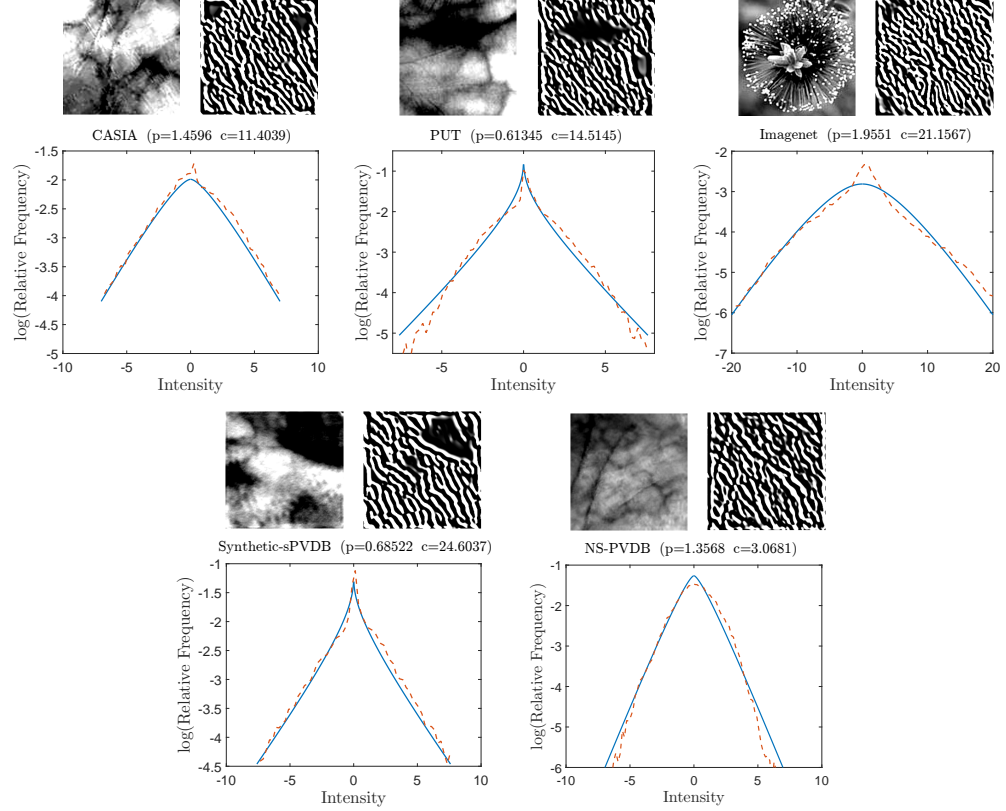


Figure 13: Comparison between real (first row) and synthetic (second row) samples using the Bessel K-forms. Each sub-image shows the original sample, the filtered image, and the corresponding curve of pixel density. Continuous and discrete trace curves represent the estimated K-forms and observed density functions from each image, respectively.

Section 2.2. As for the value of the c parameter, in [169] they show that it is not relevant since it essentially represents a scale parameter related to the range of pixel values in the image.

Table 8: Estimated Bessel K parameters for different images from the evaluated databases. The last row corresponds to the average values and the corresponding standard deviation.

	Synthetic		Real		Natural	
sPVDB	p	c	p	c	p	c
0.6849	24.5930	1.1487	10.1912	0.6134	14.5145	1.4596
0.5273	28.6493	1.3568	3.0681	0.4633	21.5892	0.5022
1.1516	12.7055	1.2071	5.3395	0.4919	20.7747	0.3798
0.6418	15.9923	1.3568	3.0681	0.3637	29.3623	0.3906
0.2960	40.8959	1.3655	7.0201	0.3495	32.8473	1.4355
0.9113	10.9084	0.7042	13.0153	0.3112	44.0356	0.6174
0.8797	10.9918	0.7032	12.2776	0.5808	19.0018	0.7953
0.5773	35.3900	0.8982	7.2657	0.3233	35.5480	0.5964
0.3800	36.2374	1.0111	7.9521	0.2980	40.1542	0.4522
0.6298	15.8142	0.9391	7.6821	0.3852	34.7648	1.3945
0.67 (\pm 0.26)	23.22 (\pm 11.45)	1.07 (\pm 0.26)	7.69 (\pm 3.41)	0.42 (\pm 0.11)	29.26 (\pm 9.85)	0.80 (\pm 0.45)
					14.14 (\pm 7.13)	1.77 (\pm 0.94)
						64.97 (\pm 53.41)

Due to the above, using the p and c parameters is not indicative of a meaningful comparison between real and synthetic palm vein images. Hence, to quantify the difference between pairs of filtered images based on the Bessel K-forms, we explored two distance measures, the KL divergence and the L^2 -metric defined as [168]:

$$d_{KL} = \int_{IR} \log \left(\frac{f_1(x)}{f_2(x)} \right) f_1(x) dx \quad (5)$$

$$d_I = \sqrt{\int_x (f_1(x) - f_2(x))^2 dx}, \quad (6)$$

where, $f_1(x)$ and $f_2(x)$ are the functions corresponding to the K-forms of each image.

The distances defined above allow to compare and classify the Bessel K-forms of the three groups of evaluated images: synthetic, real, and natural, as well as in [4]. Thus, the distance matrices among different types of images were calculated, and we performed a hierarchical clustering. Figures 14 and 15 depict the resulting dendrogram plots obtained from the classification of images of the Synthetic-sPVDB and NS-PVDB databases, respectively. In the plots, indices 1-8 denote real images taken from CASIA and PUT databases, 9-16 represent synthetic images, and 17-24 correspond to natural images. It can be noticed that real and synthetic images are clearly distinguished from natural images in all cases. Moreover, real and synthetic images are grouped into similar branches.

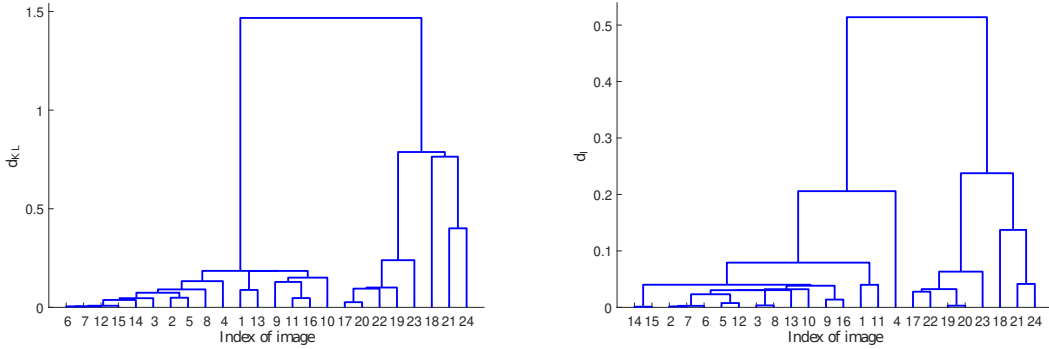


Figure 14: Clustering dendrogram plot of the distance measures d_{KL} (left) and d_I (right) obtained from the classification of images of public datasets (1-8), Synthetic-sPVDB database (9-16), and natural images of Imagenet database (17-24).

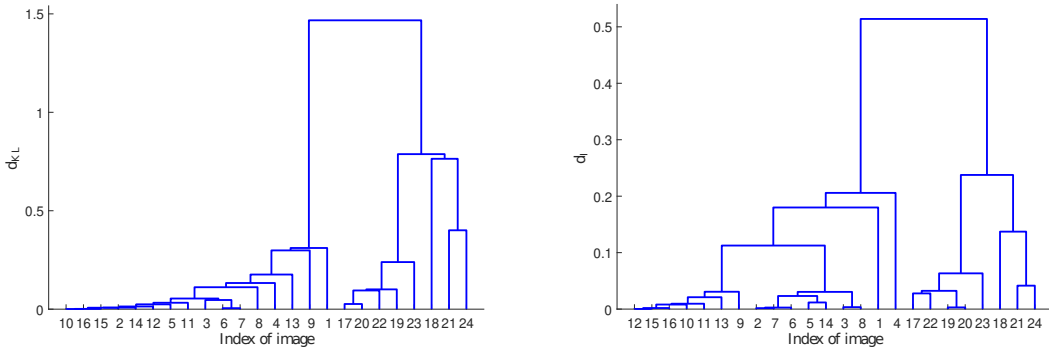


Figure 15: Clustering dendrogram plot of the distance measures d_{KL} (left) and d_I (right) obtained from the classification of images of public datasets (1-8), NS-PVDB database (9-16), and natural images of Imagenet database (17-24).

5.3.3 Quantitative evaluation

In this section, we quantitatively evaluate the proposed synthetic databases against the most representative public datasets of the state-of-the-art. For this purpose, we used quantitative measures to estimate the differences in the feature space, which is more useful than the pixel space for biometric tasks. Since the databases have different sizes, we randomly sample the 10% of images from each of them for comparison. The images were represented in the feature space using the final activations of an Inception model [171].

First, we computed the FID metric [166] to measure the statistical difference between the distributions of feature vectors. The image features are modeled using multidimensional Gaussian distributions $\mathcal{N}(\mu, \Sigma)$ with mean μ and covariance Σ . Thus, let x be a set of real images and g be a set of generated images, the $FID(x, g)$ is computed as follows:

$$FID(x, g) = \|\mu_x - \mu_g\|_2^2 + \text{Tr}(\Sigma_x + \Sigma_g - 2(\Sigma_x \Sigma_g)^{\frac{1}{2}}), \quad (7)$$

where Tr is trace operator defined as the sum of all the diagonal elements. In the case of our proposed databases, the FID metric is fundamental since it is a standard for evaluating the quality of images generated by GAN models. The lower the FID value, the better the quality and diversity of the generated images.

Besides, we computationally replicate the visual inspection experiment described in Section 5.3.1 implementing a binary classifier. Therefore, we used a 1-Nearest Neighbour (NN) classifier with a Leave-One-Out (LOO) scheme as a simple method to classify real and synthetic samples. In this case, it is expected that the closer the Accuracy is to 50%, the greater the similarity of the synthetic images are against real ones. In addition to the classification accuracy, we applied the PRD method proposed in [167] to compute the precision ($F_{1/8}$) and recall (F_8) metrics based on the feature distributions. These metrics allow the evaluation of GAN-based models complementing the FID metric. The main idea is to quantify how much of the real distribution can be generated by a part of the synthetic distribution and vice-versa.

Table 9 shows the results of quantitative evaluation of both generated databases against the most representative state-of-the-art public datasets. The obtained results suggest that the synthetic images perform better for specific databases depending on the generation procedure. Thus, Synthetic-sPVDB is closely related to CASIA-940 due to the Style-VIG process was trained with images from CASIA-850. On the other hand, NS-PVDB has more similarities to PUT and VERA datasets because their images visualize the vein patterns more clearly. These results are also consistent with the visual inspection performed.

Table 9: Results of quantitative evaluation of both generated databases (a) Synthetic-sPVDB and (b) NS-PVDB, against the most representative public datasets of the state-of-the-art.

Real Dataset	Synthetic-sPVDB				NS-PVDB			
	FID	Accuracy	F_8	$F_{1/8}$	FID	Accuracy	F_8	$F_{1/8}$
CASIA-940 [55]	67.54	0.604	0.897	0.898	227.41	0.841	0.295	0.318
PolyU [56]	103.60	0.665	0.743	0.834	203.60	0.815	0.348	0.322
PUT [64]	209.11	0.896	0.368	0.309	71.92	0.719	0.641	0.737
VERA [48]	93.01	0.637	0.750	0.844	93.01	0.634	0.825	0.865
Tongji [58]	88.91	0.621	0.853	0.862	153.01	0.714	0.403	0.447
IITI [62]	97.18	0.664	0.727	0.814	137.01	0.672	0.371	0.386

6 Discussion, Challenges, and Future Research Directions

6.1 Discussion and Main Challenges

The identification of people by palm veins provides a high level of security since the vascular structure is not exposed to the environment, and the hands generally remain in a half-open state. Compared to the veins of the fingers or the veins of the back of the hand, the palm has complex vascular patterns that generate many differentiating characteristics for personal identification. On the other hand, within the current context of Covid-19, the contactless devices that this biometry uses have been a hygienic and non-invasive solution that promotes a high level of acceptance by the user.

The main disadvantage of palm vein biometry is associated with the reduced number of subjects in public databases because they avoid the evaluation of the reliability and scalability of biometric recognition algorithms [2]. Therefore, in this paper, we review the parameters related to the acquisition devices, soft biometrics, and the anatomy of the palm veins to deepen the generation of synthetic images of the veins of the palm. From this perspective, the construction of a large-scale palm vein database using synthetic imaging mainly faces three challenges, which are described below:

- (i) **Vascular structure:** the vascular networks of the hand have complex patterns to ensure blood flow in the event of any movement. However, the multiple factors involved in obtaining images allow only the capturing of discontinuous patterns that avoid the complete segmentation of the network and its respective structural analysis. There are imaging techniques such as magnetic resonance angiography or hyperspectral images to visualize vein networks with greater precision. Despite that, these techniques are expensive and therefore not feasible to produce a biometric database and establish structural relationships. Consequently, to reproduce the vascular structure of the palm, theoretical knowledge associated with the anatomy of the arterial network and

the venous network is required. The arterial part has a branched structure described in detail, but the venous part is only described as a random network that obeys optimization principles.

- (ii) Palm texture: to reproduce the palm texture, factors associated with the acquisition devices that produce variation in brightness and contrast must be considered. Several aspects influence this variability: soft biometrics, local contrast, and lighting conditions. Soft biometrics such as gender, age, body build, and ethnicity impact in the NIR lighting response [44, 46, 172, 47]. Among the public databases, only the VERA database collects extra information about the sex and age of the individuals, which limits the study of these factors on the variability of the image. On the other hand, local contrast occurs for different reasons; among these are the different aesthetic units of the palm, the marks or defects on the skin, and the hand's position at the time of image capture. Finally, lighting conditions such as the NIR spectrum, environmental factors, body temperature, and light intensity directly affect the acquisition of the palm vein pattern since they generally produce low contrast, high noise level, and uneven lighting. It should be noted that both the variation of the power and the variation of the NIR spectrum from one acquisition device to another produce a non-standardized technology and the generation of images with different qualities.
- (iii) Quality of palm vein images: a synthetic database of palm veins should guarantee that the intra-class and inter-class variabilities are in a quality range that allows the evaluation of the reliability and robustness of the biometric recognition algorithms. In real images of palm veins, the evaluation of the quality ranges has been poorly studied, and consequently, there is not yet a standard that defines them. Regarding the works related to quality evaluation, these are limited to the analysis of self-created images and not the available public databases. Therefore, it avoids establishing a quality range that allows the scientific community to compare the robustness of the developed systems.

In Section 4.1 the existing models that allow the generation of synthetic images for biometric purposes were described. According to the review considered in this article, the models can be classified into texture methods and structural methods. The texture methods consider probability functions to reproduce the different gray levels of the images. These models are used in the augmentation of samples and not in the generation of new images, which tends to work with verification algorithms rather than identification algorithms. In contrast to the above, structural models generate new images by reproducing properties of the vascular network and the effects of acquisition devices. The importance of structural models is that they allow the evaluation of identification algorithms. Regarding the existing structural models, only the works developed in [13, 4] simulate vein images of the back of the hand and fingers, sharing similarities with palm vein images. However, the palm has more details at the level of vascular structure and palm texture, which obstructs their respective simulation.

Given the lack of knowledge of the palm vein structure, in Section 4.2, the different models that allow the generation of biological networks were reviewed in order to establish analogies with the structures found in the palm. Two types of structures are distinguished in biological networks: 1) open structures, responsible for the main nutrient supply, and 2) closed structures, responsible for fault-tolerant flow. Although there are different methods to generate these structures, they have been mainly inspired by the growth of tumors, the development of the leaves veins, or the growth of some unicellular organisms. Among the applications of these models are retinal veins, venation of insect wings, and topological optimization for heat flow; however, none of the existing models have been used to simulate palm vein structures. Despite that, the existing models could be adapted by means of appropriate parameters that make it possible to simulate the characteristics of the venous network of the palm.

In Table 10, we present a classification of existing models depending on the generation of vascular networks based on the arterial and venous structure of the palm. Models based on reaction-diffusion and diffusion-limited aggregation only allow the generation of venous structures since the bifurcations of the network cannot be controlled because they arise from random processes. The CCO algorithm would only allow generating the superficial arterial structures of the palm because the network is obtained by adding segments guided by an optimization objective that depends on the pressure or flow at the network terminations, which avoids the formation of loops that are characteristic of the venous network. The remaining models can generate both types of structure. However, they have disadvantages in reproducing palm vein patterns, except pathfinding with adaptive dynamics search, spatial colonization algorithm, and hybrids methods, because the parameters used in the growth of the network can be redefined to generate a venous pattern with an appropriate shape and besides consider optimality principles. On the other hand, the active shape needs good quality images to reproduce each network. The *Lindenmayer system* and *Particle system* can produce random structures associated with the venous network, but they do not take optimization principles into account. Although it was clear that the *Lindenmayer systems* also generate fractal structures that can be associated with genetic development, they do not allow the modeling of environmental conditions. Therefore, the most suitable models are pathfinding with adaptive dynamics search, spatial colonization algorithm, and hybrids methods, as they allow for the generation of both types of vascular networks. Finally, the B-spline-based vascular models are a technique that allows efficient point

joining with the characteristic that the resulting curve is differentiable at all points, thus providing images with a high degree of realism. Thus, it could be a good combination with the previous models.

Table 10: Classification of existing models depending on the generation of vascular networks of the hand.

Model	Arterial structure (known)	Venous structure (random)
Reaction-diffusion [115]	No	Yes
Pathfinding with adaptive dynamics [119]	Yes	Yes, (Optimal shape)
Constrained Constructive Optimization [120]	Yes	No
Diffusion-limited aggregation [126]	No	Approximate
Active shape [124]	Yes	Yes
Particle system [130]	Yes	Approximate
Lindenmayer system [132]	Yes, radial part (fractal shape)	Yes, fractal shape
Space colonization algorithm [30]	Yes	Yes
Hybrid [135, 136]	Yes	Yes
B-spline based vascular structures [137, 138]	Yes	Yes

Based on previous works and the review of the state-of-the-art, in Section 5 we introduced a general flowchart for the creation of a synthetic palm vein database. The presented model has three key foundations: (1) the vein image generator process can be implemented using different approaches depending on the parameters involved; (2) the scheme considers a uniqueness discriminator based on similarity matching, which allows the continuous growth of the biometric database; and (3) several samples per each individual comprise the generated database by applying random transformations to simulate natural variations of the acquisition process. Additionally, two generalist approaches for creating synthetic palm vein images were examined. The conducted analysis provides valuable support for the present review and strengthens the knowledge foundation for future research in this area.

The first approach consists of generating palm vein images using the StyleGAN2 architecture. Data augmentation was performed before training the network to prevent any generated sample from being rejected by the discriminator due to overfitting. However, the generator would also learn to produce the augmented data distribution that may not correspond to the real images. Hence, other generative models such as different GAN architectures or the VQ-VAE model should be evaluated to code more complex characteristics related to palm vein patterns. In the second approach, texture and vascular structure are independently generated and then fused. The vascular network is generated through a nature-based optimization process, which may not correspond to the real palm vein structure. Although both approaches validate the idea for the generation of synthetic palm images, they do not consider specific characteristics of the palm vascular structure. Therefore, they only represent the initial milestone towards developing more complex methods, which allow the generation of vein images considering the multiple parameters influencing the visualization of vein patterns. Furthermore, the computation time increases as the data increases due to the individual discriminator when constructing a large-scale database. Thus, parallel and distributed computing must be considered to implement the IUD process.

Finally, in Section 2.2, we analyze that palm vein acquisition devices are sensitive to soft traits of people, so it is necessary to consider them in the generation of synthetic images. Incorporating soft biometrics would benefit image realism and improve the evaluation performance of recognition algorithms. However, to the best of our knowledge, studies associated with the influence of soft biometrics on vein pattern visualization are very preliminary, and these studies do not allow for accurate parameter estimation for their respective simulation. Going deeper into the influence of soft biometrics requires databases containing this type of information. Therefore, further and more in-depth studies could be conducted to estimate appropriate parameters and consider them in the generation model through certain state variables that evaluate the variability of the visualization of vein patterns.

6.2 Future Research Directions

According to the problems faced by vascular-based biometrics and the generation of synthetic palm vein images, from our humble perspective, the following lines of investigation can be considered by the research community:

- (i) Knowledge of the vascular network: Considering that the structure of the palm vein network is not known in detail and that the images used in biometric recognition only provide discontinuous patterns of the vascular network, it is necessary to deepen its characterization to establish parameters that allow the network modeling. This characterization would also allow the total reconstruction of the network in the images, which would improve, among other things, the performance of the biometric recognition algorithms.

- (ii) Construction of databases that incorporate soft biometrics: The development of databases that collect extra information such as gender, age, medical conditions, etc., would allow a detailed study of its influence on the visualization of palm veins. These studies could improve the quality of the images since there would be criteria for adjusting the lighting parameters of the acquisition devices. In addition, this extra information from the images of the palm veins will allow the creation of soft biometric recognition models and multitasking biometric recognition, which could be used for other types of applications, such as for non-invasive health studies.
- (iii) Image quality evaluation: Regarding the problem associated with the lack of a quality evaluation standard for palm vein images, it is required to analyze the quality of images from public databases and define the range of variability both intra-class and inter-class to provide a reference framework available to the scientific community.
- (iv) Cross-spectral matching: due to the non-standardization of palm vein acquisition methods, there is a need to propose robust algorithms at different wavelengths of NIR illumination to recognize people regardless of the NIR spectral band used in the captured image.
- (v) Modeling synthetic images of palm veins: It is necessary to consider factors that affect the representation of vein patterns to guarantee the realism of the images generated. First, an algorithm must be proposed that reproduces the vascular structure of the palm, for which we could consider variants of the existing vascular network models studied in Section 4. On the other hand, it is required to reproduce the texture of the palm, which could be done using generative models, taking into account the effects generated by the acquisition devices and the variability of the quality of the images.
- (vi) Creation of large-scale databases: With the problems associated with the limited number of individuals in public databases, the simulation of the vascular network of the palm based on the anatomy and the simulation of the effects produced by the acquisition systems would allow developing a database of synthetic images using the proposed scheme in Figure 8. It would allow the evaluation of palm vein biometric systems on a large scale.

7 Conclusions

The objective of our study was to address the problems associated with the limited number of images in public databases, which prevent the evaluation of the reliability and scalability of large-scale palm vein recognition algorithms. To address this problem, the present work analyzed different approaches of the state-of-the-art for the generation of vascular structures, allowing to establish the main limitations and advantages of the methods studied for the generation of the vascular network of the palm. The study was carried out from a mixed approach that analyzed both the factors that influence the representation of real palm vein images and the modeling of synthetic images of vascular structures.

Regarding the representation of the images of vein patterns, the anatomy of the palm veins was taken into account to determine geometric and topological characteristics that allow the generation of realistic vascular structures. In addition, we studied the factors that influence capturing the palm vein images and their quality evaluation to guarantee that the intra-class and inter-class variability are equivalent to the real images. Regarding the modeling of vascular structures, we reviewed the models reported in the literature to determine their flexibility to produce different structures that could be used in the generation of the vascular networks of the palm. Furthermore, we formalized a general scheme for the creation of a synthetic palm vein database.

Our study made it possible to identify the main challenges facing the generation of synthetic images of palm veins. By studying the models, it was possible to establish their advantages for the generation of the arterial and venous structure of the palm for biometric purposes. The evaluation of the proposed scheme for generating a large-scale synthetic database allowed validating the proposal's effectiveness and creating the largest palm vein databases of the state-of-the-art. Based on our findings, possible lines of research around the studied problem were proposed. Due to the limits of our perspectives, the suggestions we mentioned about future research are only for reference so that they could be enriched considering the comments and experience of the scientific community.

Acknowledgments

This work was funded by the National Agency for Research and Development (ANID), Scholarship Program, Doctorado Becas Chile, 2022-21220765. R.H.-G. thanks to the Research Project ANID FONDECYT Iniciación en Investigación 2022 No. 11220693 “End-to-end multi-task learning framework for individuals identification through palm vein patterns”. The authors of the paper also thank to the Research Project FONDECYT REGULAR 2020 No. 1200810

“Very Large Fingerprint Classification based on a Fast and Distributed Extreme Learning Machine”. Portions of the research in this paper used the CASIA-MS-PalmprintV1 collected by the Chinese Academy of Sciences’ Institute of Automation (CASIA). Portions of the research in this paper used the VERA-Palmvein Corpus made available by the Idiap Research Institute, Martigny, Switzerland.

References

- [1] Anil Jain, Arun Ross, and Salil Prabhakar. An introduction to biometric recognition. *IEEE Transactions on circuits and systems for video technology*, 14(1):4–20, 2004.
- [2] Wei Wu, Stephen Elliott, Sen Lin, Shenshen Sun, and Yandong Tang. Review of palm vein recognition. *IET Biometrics*, 9(1):1–10, 2019.
- [3] Kashif Shaheed, Aihua Mao, Imran Qureshi, Munish Kumar, Sumaira Hussain, and Xingming Zhang. Recent advancements in finger vein recognition technology: Methodology, challenges and opportunities. *Information Fusion*, 79:84–109, 2022.
- [4] Fieke Hillerström, Ajay Kumar, and Raymond Veldhuis. Generating and analyzing synthetic finger vein images. In *2014 International Conference of the Biometrics Special Interest Group (BIOSIG)*, pages 1–9. IEEE, 2014.
- [5] Li Xueyan and Guo Shuxu. *The fourth biometric-vein recognition*. INTECH Open Access Publisher, 2008.
- [6] Runbin Cai and Dewen Hu. Image fusion of palmpprint and palm vein: Multispectral palm image fusion. In *2010 3rd International Congress on Image and Signal Processing*, volume 6, pages 2778–2781. IEEE, 2010.
- [7] M Rajalakshmi, R Rengaraj, and PG Student. Biometric authentication using near infrared images of palm dorsal vein patterns. *International Journal of Advanced Engineering Technology*, 2(IV):384–389, 2011.
- [8] Olegs Nikisins, Modris Greitans, Rihards Fuksis, Mihails Pudzs, and Zanda Serzane. Increasing the reliability of biometric verification by using 3d face information and palm vein patterns. *BIOSIG 2010: Biometrics and Electronic Signatures. Proceedings of the Special Interest Group on Biometrics and Electronic Signatures*, 2010.
- [9] Gunjan Shah, Sagar Shirke, Sonam Sawant, and Yogesh H Dandawate. Palm vein pattern-based biometric recognition system. *International Journal of Computer Applications in Technology*, 51(2):105–111, 2015.
- [10] Mustafa Cömert and Ali Yıldız. Palm Vein Authentication and Verification System. *Acta Physica Polonica A*, 130(1):175–177, 2016.
- [11] Paul E Kilgore, SHI Weisong, Jie Cao, Zhifeng Yu, and XU Mingyang. Palm vein-based low-cost mobile identification system for a wide age range, April 20 2017. US Patent App. 15/293,798.
- [12] Andreas Uhl, Christoph Busch, Sébastien Marcel, and Raymond Veldhuis. *Handbook of vascular biometrics*. Springer Nature, 2020.
- [13] Septimiu Crisan, Ioan Gavril Târnovan, and TE Crisan. A hand vein structure simulation platform for algorithm testing and biometric identification. In *16th IMEKO TC4 Symposium, Florence, Italy*, 2008.
- [14] Dario Maio, Davide Maltoni, Raffaele Cappelli, Jim L Wayman, and Anil K Jain. FVC2004: Third fingerprint verification competition. In *International conference on biometric authentication*, pages 1–7. Springer, 2004.
- [15] Zhuoshi Wei, Yufei Han, Zhenan Sun, and Tieniu Tan. Palmpprint image synthesis: A preliminary study. In *2008 15th IEEE International Conference on Image Processing*, pages 285–288. IEEE, 2008.
- [16] Jinyu Zuo, Natalia A Schmid, and Xiaohan Chen. On generation and analysis of synthetic iris images. *IEEE Transactions on Information Forensics and Security*, 2(1):77–90, 2007.
- [17] Edwin Salazar, Ruber Hernández-García, Ricardo J. Barrientos, Karina Vilches, Marco Mora, and Angel Vásquez. Generating style-based palm vein synthetic images for the creation of large-scale datasets. In *11th International Conference of Pattern Recognition Systems (ICPRS 2021)*, pages 182–187(5). Institution of Engineering and Technology, 2021.
- [18] Edwin Salazar, Ruber Hernández-García, Ricardo J. Barrientos, Karina Vilches, Marco Mora, and Angel Vásquez. Automatic generation of synthetic palm vein images: a nature-based approach. In *11th International Conference of Pattern Recognition Systems (ICPRS 2021)*, pages 38–43(5). Institution of Engineering and Technology, 2021.
- [19] Jianfeng Zhang, Zhiying Lu, Min Li, and Haopeng Wu. GAN-Based Image Augmentation for Finger-Vein Biometric Recognition. *IEEE Access*, 7:183118–183132, 2019.
- [20] Hanwen Yang, Peiyu Fang, and Zhiang Hao. A GAN-Based Method for Generating Finger Vein Dataset. In *2020 3rd International Conference on Algorithms, Computing and Artificial Intelligence, ACAI 2020*. Association for Computing Machinery, 2020.

- [21] Abhijit Das, Prabir Mondal, Umapada Pal, Michael Blumenstein, and Miguel A Ferrer. Sclera vessel pattern synthesis based on a non-parametric texture synthesis technique. In *Proceedings of international conference on computer vision and image processing*, pages 241–250. Springer, 2017.
- [22] A Sukop, O Nařka, M Dušková, M Tvrdek, R Kufa, O Měšťák, and L Hauschwitcová. Clinical anatomy of the dorsal venous network in fingers with regard to replantation. *Clinical Anatomy: The Official Journal of the American Association of Clinical Anatomists and the British Association of Clinical Anatomists*, 20(1):77–81, 2007.
- [23] F. Kiss and J. Szentágothai. *Atlas anatomiae corporis humani*. Atlas d'anatomie du corps humain. Akadémiai Kiadó, 1974.
- [24] Cemil Kirbas and Francis Quek. A Review of Vessel Extraction Techniques and Algorithms. *ACM Computing Surveys*, 36(2):81–121, 2004.
- [25] Pengshuai Yin, Hongmin Cai, and Qingyao Wu. Df-net: Deep fusion network for multi-source vessel segmentation. *Information Fusion*, 78:199–208, 2022.
- [26] SMA Aghamirmohammadi, R Bozorgmehry Boozarjomehry, and M Abdekhodaie. Modelling of retinal vasculature based on genetically tuned parametric L-system. *Royal Society open science*, 5(5):1–20, 2018.
- [27] Marco Scianna, CG Bell, and Luigi Preziosi. A review of mathematical models for the formation of vascular networks. *Journal of theoretical biology*, 333:174–209, 2013.
- [28] Cassot Francis, Lauwers Frederic, Lorthois Sylvie, Puwanarajah Prasanna, and Duvernoy Henri. Scaling laws for branching vessels of human cerebral cortex. *Microcirculation*, 16(4):331–344, 2009.
- [29] Adam Runions, Martin Fuhrer, Brendan Lane, Pavol Federl, Anne-Gaëlle Rolland-Lagan, and Przemyslaw Prusinkiewicz. Modeling and visualization of leaf venation patterns. In *ACM SIGGRAPH 2005 Papers*, pages 702–711. 2005.
- [30] Adam Runions, Brendan Lane, and Przemyslaw Prusinkiewicz. Modeling Trees with a Space Colonization Algorithm. *Eurographics Workshop on Natural Phenomena*, 7:63–70, 2007.
- [31] Przemyslaw Prusinkiewicz and Adam Runions. Computational models of plant development and form. *New Phytologist*, 193(3):549–569, 2012.
- [32] Azimah Ajam, Azrina Abd Aziz, Vijanth Sagayan Asirvadam, Ahmad Sobri Muda, Ibrahima Faye, and S Jamal Safdar Gardezi. A review on segmentation and modeling of cerebral vasculature for surgical planning. *IEEE Access*, 5:15222–15240, 2017.
- [33] John J Bergan and Nisha Bunke-Paquette. *The vein book*. OXFORD University press, 2014.
- [34] Åke Nyström, Jan Fridén, and Graham D Lister. Superficial venous anatomy of the human palm. *Scandinavian Journal of Plastic and Reconstructive Surgery and Hand Surgery*, 24(2):121–127, 1990.
- [35] J.T. Hansen. *Netter's Anatomy Flash Cards E-Book*. Netter Basic Science. Elsevier Health Sciences, 2017.
- [36] SS Coleman and BJ Anson. Arterial patterns in the hand based upon a study of 650 specimens. *Plastic and Reconstructive Surgery*, 29(1):85–86, 1962.
- [37] N Jelicic, S Gajisin, and A Zbrodowski. Arcus palmaris superficialis. *Acta anatomica*, 132(3):187–190, 1988.
- [38] Nicolás Ernesto Ottone, Natalia Prum, Mario Dominguez, Esteban Blasi, Carlos Medan, Sergio Shinzato, Diana Finkelstein, and Vicente Hugo Bertone. Analysis and clinical importance of superficial arterial palmar irrigation and its variants over 86 cases. *Int J Morphol*, 28(1):157–64, 2010.
- [39] Michael J Botte. *Surgical anatomy of the hand and upper extremity*. Lippincott Williams & Wilkins, 2003.
- [40] Joon Pio Jp Hong, Donghoon Choi, and Hyunsuk Peter Suh. Perforator Flaps. In *Interventional Treatment of Wounds*, pages 153–167. Springer, 2018.
- [41] Seth R Thaller. Grabb and Smith's plastic surgery. *Plastic and Reconstructive Surgery*, 133(5):1311–1312, 2014.
- [42] Shady A Rehim, Evan Kowalski, and Kevin C Chung. Enhancing aesthetic outcomes of soft tissue coverage of the hand. *Plastic and reconstructive surgery*, 135(2):413e, 2015.
- [43] Septimiu Crisan, Joan Gavril Tarnovan, and Titus Eduard Crisan. A low cost vein detection system using near infrared radiation. In *2007 IEEE Sensors Applications Symposium*, pages 1–6. IEEE, 2007.
- [44] Zhihuai Xie, Zhenhua Guo, and Chengshan Qian. Palmprint gender classification by convolutional neural network. *IET Computer Vision*, 12(4):476–483, 2018.
- [45] Anil K Jain, Sarat C Dass, and Karthik Nandakumar. Soft biometric traits for personal recognition systems. In *International conference on biometric authentication*, pages 731–738. Springer, 2004.

- [46] Wafa Damak, Randa Boukhris Trabelsi, Alima Damak Masmoudi, and Dorra Sellami. Palm Vein Age and Gender Estimation Using Center Symmetric-Local Binary Pattern. In *International Joint Conference: 12th International Conference on Computational Intelligence in Security for Information Systems (CISIS 2019) and 10th International Conference on European Transnational Education (ICEUTE 2019)*, pages 114–123. Springer, 2019.
- [47] Gerda Edelman, Vicky Manti, Saskia M van Ruth, Ton van Leeuwen, and Maurice Aalders. Identification and age estimation of blood stains on colored backgrounds by near infrared spectroscopy. *Forensic science international*, 220(1-3):239–244, 2012.
- [48] Pedro Tome and Sébastien Marcel. Palm vein database and experimental framework for reproducible research. In *2015 International Conference of the Biometrics Special Interest Group (BIOSIG)*, pages 1–7. IEEE, 2015.
- [49] David Zabala-Blanco, Ruber Hernández-García, Ricardo J Barrientos, and Marco Mora. Evaluation of the standard and regularized elms for gender and age classification based on palm vein images. In *2021 40th International Conference of the Chilean Computer Science Society (SCCC)*, pages 1–8. IEEE, 2021.
- [50] Michał Waluś, Krzysztof Bernacki, and Jacek Konopacki. Impact of NIR wavelength lighting in image acquisition on finger vein biometric system effectiveness. *Opto-Electronics Review*, 25(4):263–268, 2017.
- [51] Leedham Wang, Graham Leedham, and S-Y Cho. Infrared imaging of hand vein patterns for biometric purposes. *IET computer vision*, 1(3):113–122, 2007.
- [52] Hengyi Zhang, Chaoying Tang, Xiaojie Li, and Adams Wai Kin Kong. A study of similarity between genetically identical body vein patterns. In *2014 IEEE Symposium on Computational Intelligence in Biometrics and Identity Management (CIBIM)*, pages 151–159. IEEE, 2014.
- [53] Yiding Wang, Qiangyu Duan, Lik-Kwan Shark, and Di Huang. Improving hand vein recognition by score weighted fusion of wavelet-domain multi-radius local binary patterns. *International Journal of Computer Applications in Technology*, 54(3):151–160, 2016.
- [54] Christof Kauba, Bernhard Prommegger, and Andreas Uhl. Combined fully contactless finger and hand vein capturing device with a corresponding dataset. *Sensors*, 19(22):5014, 2019.
- [55] Ying Hao, Zhenan Sun, Tieniu Tan, and Chao Ren. Multispectral palm image fusion for accurate contact-free palmprint recognition. In *2008 15th IEEE International Conference on Image Processing*, pages 281–284. IEEE, 2008.
- [56] David Zhang, Zhenhua Guo, Guangming Lu, Lei Zhang, and Wangmeng Zuo. An online system of multispectral palmprint verification. *IEEE transactions on instrumentation and measurement*, 59(2):480–490, 2009.
- [57] Septimiu Crisan, Ioan Gavril Tarnovan, and Titus Eduard Crisan. Radiation optimization and image processing algorithms in the identification of hand vein patterns. *Computer Standards & Interfaces*, 32(3):130–140, 2010.
- [58] Lin Zhang, Zaixi Cheng, Ying Shen, and Dongqing Wang. Palmprint and palmvein recognition based on DCNN and a new large-scale contactless palmvein dataset. *Symmetry*, 10(4):78, 2018.
- [59] Maleika Mehr Nigar M Heenaye and RK Subramanian. A study of dorsal vein pattern for biometric security. *University of Mauritius Research Journal*, 15(1):17–25, 2009.
- [60] Jingfan Fan, Jian Yang, Chan Wu, Danni Ai, Hong Song, Aimin Hao, and Yongtian Wang. Multiple Features Decomposition for Subcutaneous Vein Extraction and Measurement. *IEEE Access*, 6:11265–11277, 2018.
- [61] Fernando Costa and Italo Biaggioni. Role of nitric oxide in adenosine-induced vasodilation in humans. *Hypertension*, 31(5):1061–1064, 1998.
- [62] Shruti Bhilare, Gaurav Jaswal, Vivek Kanhangad, and Aditya Nigam. Single-sensor hand-vein multimodal biometric recognition using multiscale deep pyramidal approach. *Machine Vision and Applications*, 29(8):1269–1286, 2018.
- [63] Peng CHEN, Xiaoke LAN, Feng JIN, and Jinzhuan SHI. Research of high quality palm vein image acquisition and ROI extraction. *Chinese Journal of Sensors and Actuators*, 7(013), 2015.
- [64] R Kabaciński and M Kowalski. Vein pattern database and benchmark results. *Electronics Letters*, 47(20):1127–1128, 2011.
- [65] Marcos Faundez-Zanuy, Jiri Mekyska, and Xavier Font-Aragonès. A new hand image database simultaneously acquired in visible, near-infrared and thermal spectrums. *Cognitive Computation*, 6(2):230–240, 2014.
- [66] Önsen Toygar, Felix O Babalola, and Yiltan Bitirim. FYO: a novel multimodal vein database with palmar, dorsal and wrist biometrics. *IEEE Access*, 8:82461–82470, 2020.

- [67] Goh Kah Ong Michael, Tee Connie, Lau Siong Hoe, and Andrew Teoh Beng Jin. Design and implementation of a contactless palm vein recognition system. In *Proceedings of the 2010 Symposium on Information and Communication Technology*, SoICT '10, pages 92–99. Association for Computing Machinery, 2010.
- [68] Huan Zhang and Dewen Hu. A palm vein recognition system. In *2010 International Conference on Intelligent Computation Technology and Automation*, volume 1, pages 285–288. IEEE, 2010.
- [69] John M Irvine. National imagery interpretability rating scales (NIIRS): overview and methodology. In *Airborne Reconnaissance XXI*, volume 3128, pages 93–103. International Society for Optics and Photonics, 1997.
- [70] ISO/IEC 29794-4. Information technology – Biometric sample quality– Part 4: Finger image data. *International Standard ISO*, 2017.
- [71] ISO/IEC 29794-1. Information technology – Biometric sample quality – Part 1: Framework. *International Standard ISO*, 2016.
- [72] ISO/IEC TR 29794-5. Information technology – Biometric sample quality – Part 5: Face image data. *International Standard ISO*, 2010.
- [73] Wang Jiaqiang, Yu Ming, Qu Hanbing, and Li Bin. Analysis of palm vein image quality and recognition with different distance. In *2013 Fourth International Conference on Digital Manufacturing & Automation*, pages 215–218. IEEE, 2013.
- [74] Chunyi Wang, Xinhua Zeng, Xiongwei Sun, Wengong Dong, and Zede Zhu. Quality assessment on near infrared palm vein image. In *2017 32nd Youth academic annual conference of Chinese association of automation (YAC)*, pages 1127–1130. IEEE, 2017.
- [75] Wengong Dong, Jianwen Ren, Yahui Su, Chunyi Wang, Xiongwei Sun, Zede Zhu, and Xinhua Zeng. Research on multi-spectral adaptive method for palm vein capturing based on image quality. In *2017 32nd Youth Academic Annual Conference of Chinese Association of Automation (YAC)*, pages 1154–1157. IEEE, 2017.
- [76] Chunyi Wang, Xiongwei Sun, Wengong Dong, Zede Zhu, Shouguo Zheng, and Xinhua Zeng. Quality assessment of palm vein image using natural scene statistics. In *CCF Chinese Conference on Computer Vision*, pages 248–255. Springer, 2017.
- [77] Zhou Wang, Alan C Bovik, Hamid R Sheikh, and Eero P Simoncelli. Image quality assessment: from error visibility to structural similarity. *IEEE transactions on image processing*, 13(4):600–612, 2004.
- [78] Frederique Crete, Thierry Dolmire, Patricia Ladret, and Marina Nicolas. The blur effect: perception and estimation with a new no-reference perceptual blur metric. In *Human vision and electronic imaging XII*, volume 6492, page 64920I. International Society for Optics and Photonics, 2007.
- [79] Anish Mittal, Rajiv Soundararajan, and Alan C Bovik. Making a “completely blind” image quality analyzer. *IEEE Signal processing letters*, 20(3):209–212, 2012.
- [80] Hui Ma, Kejun Wang, Linlin Fan, and Fengpeng Cui. A finger vein image quality assessment method using object and human visual system index. In *International Conference on Intelligent Science and Intelligent Data Engineering*, pages 498–506. Springer, 2012.
- [81] Yilong Yin, Lili Liu, and Xiwei Sun. SDUMLA-HMT: a multimodal biometric database. In *Chinese Conference on Biometric Recognition*, pages 260–268. Springer, 2011.
- [82] Huafeng Qin and Mounim A El-Yacoubi. Deep representation for finger-vein image-quality assessment. *IEEE Transactions on Circuits and Systems for Video Technology*, 28(8):1677–1693, 2017.
- [83] Huafeng Qin and Mounîm A El-Yacoubi. Finger-vein quality assessment by representation learning from binary images. In *International Conference on Neural Information Processing*, pages 421–431. Springer, 2015.
- [84] Takashi Shinzaki. Use case of palm vein authentication. In *Handbook of Vascular Biometrics*, pages 145–158. Springer, 2020.
- [85] Masaki Watanabe. Palm vein authentication. In *Advances in biometrics*, pages 75–88. Springer, 2008.
- [86] Wei Jia, Jian Gao, Wei Xia, Yang Zhao, Hai Min, and Jing-Ting Lu. A Performance Evaluation of Classic Convolutional Neural Networks for 2D and 3D Palmprint and Palm Vein Recognition. *International Journal of Automation and Computing*, pages 1–27, 2021.
- [87] Kashif Shaheed, Hangang Liu, Gongping Yang, Imran Qureshi, Jie Gou, and Yilong Yin. A systematic review of finger vein recognition techniques. *Information*, 9(9):213, 2018.
- [88] Tero Karras, Samuli Laine, and Timo Aila. A style-based generator architecture for generative adversarial networks. In *Proceedings of the IEEE/CVF Conference on Computer Vision and Pattern Recognition*, pages 4401–4410, 2019.

- [89] Yuxin Liu, Chao Gao, Zili Zhang, Yuheng Wu, Mingxin Liang, Li Tao, and Yuxiao Lu. A new multi-agent system to simulate the foraging behaviors of physarum. *Natural computing*, 16(1):15–29, 2017.
- [90] Ruber Hernández-García, Sebastián Guidet, Ricardo J Barrientos, and Fernando Emmanuel Frati. Massive finger-vein identification based on local line binary pattern under parallel and distributed systems. In *2019 38th International Conference of the Chilean Computer Science Society (SCCC)*, pages 1–7. IEEE, 2019.
- [91] Ruber Hernández-García, Ricardo J Barrientos, Cristopher Rojas, and Marco Mora. Individuals Identification Based on Palm Vein Matching under a Parallel Environment. *Applied Sciences*, 9(14):2805, 2019.
- [92] S Guidet, RJ Barrientos, R Hernández-García, and FE Frati. Exhaustive similarity search on a many-core architecture for finger-vein massive identification. In *Journal of Physics: Conference Series*, volume 1702, page 012012. IOP Publishing, 2020.
- [93] Jung Yeop Lee and Sang Joon Lee. Murray’s law and the bifurcation angle in the arterial micro-circulation system and their application to the design of microfluidics. *Microfluidics and Nanofluidics*, 8(1):85, 2010.
- [94] Ulf Grenander and Anuj Srivastava. Probability models for clutter in natural images. *IEEE Transactions on Pattern Analysis and Machine Intelligence*, 23(4):424–429, 2001.
- [95] Abdul Jabbar, Xi Li, and Bourahla Omar. A survey on generative adversarial networks: Variants, applications, and training. *54*(8), 2021.
- [96] Pourya Shamsolmoali, Masoumeh Zareapoor, Eric Granger, Huiyu Zhou, Ruili Wang, M. Emre Celebi, and Jie Yang. Image synthesis with adversarial networks: A comprehensive survey and case studies. *Information Fusion*, 72:126–146, 2021.
- [97] Jun-Yan Zhu, Taesung Park, Phillip Isola, and Alexei A Efros. Unpaired image-to-image translation using cycle-consistent adversarial networks. In *Proceedings of the IEEE international conference on computer vision*, pages 2223–2232, 2017.
- [98] Justin Johnson, Alexandre Alahi, and Li Fei-Fei. Perceptual losses for real-time style transfer and super-resolution. In *European conference on computer vision*, pages 694–711. Springer, 2016.
- [99] Phillip Isola, Jun-Yan Zhu, Tinghui Zhou, and Alexei A Efros. Image-To-Image Translation With Conditional Adversarial Networks. In *Proceedings of the IEEE Conference on Computer Vision and Pattern Recognition*, pages 1125–1134, 2017.
- [100] Yu Lu, Shan Juan Xie, Sook Yoon, Zhihui Wang, and Dong Sun Park. An available database for the research of finger vein recognition. In *2013 6th International congress on image and signal processing (CISP)*, volume 1, pages 410–415. IEEE, 2013.
- [101] Alexei A Efros and Thomas K Leung. Texture synthesis by non-parametric sampling. In *Proceedings of the seventh IEEE international conference on computer vision*, volume 2, pages 1033–1038. IEEE, 1999.
- [102] Hugo Proen  a and Lu  s A Alexandre. Ubiris: A noisy iris image database. In *International Conference on Image Analysis and Processing*, pages 970–977. Springer, 2005.
- [103] Werner Baumgarten, Tetsuo Ueda, and Marcus JB Hauser. Plasmodial vein networks of the slime mold Physarum polycephalum form regular graphs. *Physical Review E*, 82(4):046113, 2010.
- [104] Arya Krishnan, Gayathri R. Nayar, Tony Thomas, and N. Ake Nystrom. Feba - an anatomy based finger vein classification. In *2020 IEEE International Joint Conference on Biometrics (IJCB)*, pages 1–9, 2020.
- [105] Ruber Hernández-García, Jos   I Santamar  a, Ricardo J Barrientos, Edwin H Salazar-Jurado, Francisco Manuel Castro, Juli  n Ramos-C  zar, and Nicol  s Guil. Large-scale palm vein recognition on synthetic datasets. In *2021 40th International Conference of the Chilean Computer Science Society (SCCC)*, pages 1–8. IEEE, 2021.
- [106] Han Zhang, Ian Goodfellow, Dimitris Metaxas, and Augustus Odena. Self-attention generative adversarial networks. In *International conference on machine learning*, pages 7354–7363. PMLR, 2019.
- [107] Alec Radford, Luke Metz, and Soumith Chintala. Unsupervised representation learning with deep convolutional generative adversarial networks. *arXiv preprint arXiv:1511.06434*, 2015.
- [108] Geoffrey B West, James H Brown, and Brian J Enquist. A general model for the origin of allometric scaling laws in biology. *Science*, 276(5309):122–126, 1997.
- [109] Jayanth R Banavar, Amos Maritan, and Andrea Rinaldo. Size and form in efficient transportation networks. *Nature*, 399(6732):130–132, 1999.
- [110] Peter Sheridan Dodds. Optimal form of branching supply and collection networks. *Physical review letters*, 104(4):048702, 2010.

- [111] Dan Hu and David Cai. Adaptation and optimization of biological transport networks. *Physical review letters*, 111(13):138701, 2013.
- [112] Francis Corson. Fluctuations and redundancy in optimal transport networks. *Physical Review Letters*, 104(4):048703, 2010.
- [113] Eleni Katifori, Gergely J Szöllősi, and Marcelo O Magnasco. Damage and fluctuations induce loops in optimal transport networks. *Physical review letters*, 104(4):048704, 2010.
- [114] LinGen Chen. Progress in study on constructal theory and its applications. *Science China Technological Sciences*, 55(3):802–820, 2012.
- [115] Alan Mathison Turing. The chemical basis of morphogenesis. *Bulletin of Mathematical Biology*, 52(1):153–197, 1990.
- [116] H Meinhardt et al. Morphogenesis of lines and nets. *Differentiation*, 6(2):117–123, 1976.
- [117] Shigeru Kondo and Takashi Miura. Reaction-diffusion model as a framework for understanding biological pattern formation. *science*, 329(5999):1616–1620, 2010.
- [118] Atsushi Tero, Ryo Kobayashi, and Toshiyuki Nakagaki. Physarum solver: A biologically inspired method of road-network navigation. *Physica A: Statistical Mechanics and its Applications*, 363(1):115–119, 2006.
- [119] Jeff Jones. Characteristics of pattern formation and evolution in approximations of Physarum transport networks. *Artificial Life*, 16(2):127–153, 2010.
- [120] RAB de Queiroz, PJ Blanco, RA Feijóo, and JN Ulysses. Constructive algorithm of optimized arterial networks. In *VI Latin American Congress on Biomedical Engineering CLAIB 2014, Paraná, Argentina 29, 30 & 31 October 2014*, pages 884–887. Springer, 2015.
- [121] Anh V Bui, Richard Manasseh, Kurt Liffman, and Ilija D Šutalo. Development of optimized vascular fractal tree models using level set distance function. *Medical engineering & physics*, 32(7):790–794, 2010.
- [122] Gonzalo Daniel Maso Talou, Soroush Safaei, Peter John Hunter, and Pablo Javier Blanco. Adaptive constrained constructive optimisation for complex vascularisation processes. *Scientific Reports*, 11(1):1–22, 2021.
- [123] Satoshi Ii, Hiroki Kitade, Shunichi Ishida, Yohsuke Imai, Yoshiyuki Watanabe, and Shigeo Wada. Multiscale modeling of human cerebrovasculature: A hybrid approach using image-based geometry and a mathematical algorithm. *PLoS Computational Biology*, 16(6):e1007943, 2020.
- [124] Timothy F Cootes, Christopher J Taylor, David H Cooper, and Jim Graham. Active shape models-their training and application. *Computer vision and image understanding*, 61(1):38–59, 1995.
- [125] Lorenza Bonaldi, Elisa Menti, Lucia Ballerini, Alfredo Ruggeri, and Emanuele Trucco. Automatic generation of synthetic retinal fundus images: vascular network. *Procedia Computer Science*, 90:54–60, 2016.
- [126] Thomas Witten and Leonard Sander. Diffusion-Limited Aggregation, a Kinetic Critical Phenomenon. *Physical Review Letters*, 47(19):1400–1403, 1981.
- [127] Paul Bourke. Constrained diffusion-limited aggregation in 3 dimensions. *Computers & Graphics*, 30(4):646–649, 2006.
- [128] Jon Pelletier and Donald Turcotte. Shapes of river networks and leaves: are they statistically similar? *Philosophical Transactions of the Royal Society of London. Series B: Biological Sciences*, 355(1394):307–311, 2000.
- [129] Jonathan C Roberts. Sticky pixels: Evolutionary growth by random drop ballistic aggregation. In *Eurographics UK 2001 Conference Proceedings*, pages 149–155. Eurographics, 2001.
- [130] Yodthong Rodkaew, Suchada Siripant, Chidchanok Lursinsap, and Prabhas Chongstitvatana. An algorithm for generating vein images for realistic modeling of a leaf. In *Proceedings of the international conference on computational mathematics and modeling*, volume 9, pages 1–9, 2002.
- [131] Danny J Lohan, Ercan M Dede, and James T Allison. Topology optimization for heat conduction using generative design algorithms. *Structural and Multidisciplinary Optimization*, 55(3):1063–1077, 2017.
- [132] Przemyslaw Prusinkiewicz. Art and science of life: designing and growing virtual plants with L-systems. In *XXVI International Horticultural Congress: Nursery Crops; Development, Evaluation, Production and Use 630*, pages 15–28, 2002.
- [133] Miguel A Galarreta-Valverde, Maysa MG Macedo, Choukri Mekkaoui, and Marcel P Jackowski. Three-dimensional synthetic blood vessel generation using stochastic L-systems. In *Medical Imaging 2013: Image Processing*, volume 8669, page 86691I. International Society for Optics and Photonics, 2013.

- [134] A Ruiz-Sobrino, CA Martín-Blanco, Tomás Navarro, Isabel Almudi, Giulio Masiero, M Jiménez-Caballero, DB Buchwalter, DH Funk, JL Gattoliat, María C Lemos, et al. Space colonization by branching trachea explains the morphospace of a simple respiratory organ. *Developmental biology*, 462(1):50–59, 2020.
- [135] Wenbiao Jin, Wenzhe Gu, and Zhifeng Zhang. An improved method for modeling of leaf venation patterns. In *2009 2nd International Congress on Image and Signal Processing*, pages 1–5. IEEE, 2009.
- [136] S Salcedo-Sanz and L Cuadra. Hybrid L-systems–diffusion limited aggregation schemes. *Physica A: Statistical Mechanics and its Applications*, 514:592–605, 2019.
- [137] Jie Li, William C Regli, and Wei Sun. Mathematical representation of the vascular structure and applications. In *Proceedings of the 2007 ACM symposium on Solid and physical modeling*, pages 373–378, 2007.
- [138] Dario Lo Castro, Domenico Tegolo, and Cesare Valenti. A visual framework to create photorealistic retinal vessels for diagnosis purposes. *Journal of Biomedical Informatics*, 108:103490, 2020.
- [139] Alexander RA Anderson and Mark A J Chaplain. Continuous and discrete mathematical models of tumor-induced angiogenesis. *Bulletin of mathematical biology*, 60(5):857–899, 1998.
- [140] A Gamba, D Ambrosi, A Coniglio, A De Candia, S Di Talia, Enrico Giraudo, Guido Serini, Luigi Preziosi, and Federico Bussolino. Percolation, morphogenesis, and burgers dynamics in blood vessels formation. *Physical review letters*, 90(11):118101, 2003.
- [141] Rebecca J Shipley, Amy F Smith, Paul W Sweeney, Axel R Pries, and Timothy W Secomb. A hybrid discrete–continuum approach for modelling microcirculatory blood flow. *Mathematical medicine and biology: a journal of the IMA*, 37(1):40–57, 2020.
- [142] Valentina Lanza, Davide Ambrosi, and Luigi Preziosi. Exogenous control of vascular network formation in vitro: a mathematical model. *Networks & Heterogeneous Media*, 1(4):621, 2006.
- [143] Hans Meinhardt. Models of Biological Pattern Formation: From Elementary Steps to the Organization of Embryonic Axes. *Current Topics in Developmental Biology*, 81:1–63, 2008.
- [144] Henrik Jönsson and Paweł Krupinski. Modeling plant growth and pattern formation. *Current opinion in plant biology*, 13(1):5–11, 2010.
- [145] Mohsen Dorraki, Anahita Fouladzadeh, Andrew Allison, Claudine S Bonder, and Derek Abbott. Angiogenic Networks in Tumors—Insights via Mathematical Modeling. *IEEE Access*, 8:43215–43228, 2020.
- [146] Omar Serrano-Pérez, Miguel G Villarreal-Cervantes, Juan C González-Robles, and Alejandro Rodríguez-Molina. Meta-heuristic algorithms for the control tuning of omnidirectional mobile robots. *Engineering Optimization*, 52(2):325–342, 2019.
- [147] Zahra Beheshti and Siti Mariyam Hj Shamsuddin. A review of population-based meta-heuristic algorithms. *Int. J. Adv. Soft Comput. Appl.*, 5(1):1–35, 2013.
- [148] Richard W and Burkhardt J. Lamarck, evolution, and the inheritance of acquired characters. *Genetics*, 194(4):793–805, 2013.
- [149] Dai Akita. *Study on biological transport network utilizing plasmodium of Physarum polycephalum*. PhD thesis, Hokkaido University, 2017.
- [150] Wolfgang Schreiner, Martin Neumann, Friederike Neumann, Susanne M Roedler, Adelheid End, P Buxbaum, Michael R Müller, and Paul Spieckermann. The branching angles in computer-generated optimized models of arterial trees. *The Journal of general physiology*, 103(6):975–989, 1994.
- [151] Wolfgang Schreiner, Friederike Neumann, Martin Neumann, Adelheid End, and Susanne M Roedler. Anatomical variability and functional ability of vascular trees modeled by constrained constructive optimization. *Journal of theoretical biology*, 187(2):147–158, 1997.
- [152] Manfred Georg, Tobias Preusser, and Horst K Hahn. Global constructive optimization of vascular systems. 2010.
- [153] Vladas Sidoravicius and Alexandre Stauffer. Multi-particle diffusion limited aggregation. *Inventiones mathematicae*, 218(2):491–571, 2019.
- [154] MY Lin, HM Lindsay, DA Weitz, RC Ball, R Klein, and P Meakin. Universality of fractal aggregates as probed by light scattering. In *Fractals in the Natural Sciences*, pages 71–88. Princeton University Press, 2014.
- [155] Naman Kohli, Daksha Yadav, Mayank Vatsa, Richa Singh, and Afzel Noore. Synthetic iris presentation attack using iDCGAN. In *2017 IEEE International Joint Conference on Biometrics (IJCB)*, pages 674–680. IEEE, 2017.

- [156] Shivangi Yadav, Cunjian Chen, and Arun Ross. Synthesizing Iris Images using RaSGAN with Application in Presentation Attack Detection. In *Proceedings of the IEEE Conference on Computer Vision and Pattern Recognition Workshops*, pages 0–0, 2019.
- [157] Chao Yang and Ser-Nam Lim. One-Shot Domain Adaptation For Face Generation. In *Proceedings of the IEEE/CVF Conference on Computer Vision and Pattern Recognition*, pages 5921–5930, 2020.
- [158] Viktor Varkarakis, Shabab Bazrafkan, and Peter Corcoran. Re-Training StyleGAN - A First Step Towards Building Large, Scalable Synthetic Facial Datasets. pages 1–6, 2020.
- [159] Tero Karras, Samuli Laine, Miika Aittala, Janne Hellsten, Jaakko Lehtinen, and Timo Aila. Analyzing and Improving the Image Quality of StyleGAN. In *Proceedings of the IEEE/CVF Conference on Computer Vision and Pattern Recognition*, pages 8110–8119, 2020.
- [160] Atsushi Tero, Ryo Kobayashi, and Toshiyuki Nakagaki. A mathematical model for adaptive transport network in path finding by true slime mold. *Journal of theoretical biology*, 244(4):553–564, 2007.
- [161] Yukio-Pegio Gunji, Tomohiro Shirakawa, Takayuki Niizato, and Taichi Haruna. Minimal model of a cell connecting amoebic motion and adaptive transport networks. *Journal of theoretical biology*, 253(4):659–667, 2008.
- [162] Pascal Gwosdek, Sven Grawenig, Andrés Bruhn, and Joachim Weickert. Theoretical foundations of gaussian convolution by extended box filtering. In *International Conference on Scale Space and Variational Methods in Computer Vision*, pages 447–458. Springer, 2011.
- [163] Robert M Haralick, Karthikeyan Shanmugam, and Its' Hak Dinstein. Textural features for image classification. *IEEE Transactions on systems, man, and cybernetics*, (6):610–621, 1973.
- [164] Keyan Ding, Kede Ma, Shiqi Wang, and Eero P Simoncelli. Image quality assessment: Unifying structure and texture similarity. *arXiv preprint arXiv:2004.07728*, 2020.
- [165] Zhou Wang y AC Bovik y HR Sheikh y EP Simoncelli. Image quality assessment: from error visibility to structural similarity. *IEEE Transactions on Image Processing*, 13(4):600–612, 2004.
- [166] Martin Heusel, Hubert Ramsauer, Thomas Unterthiner, Bernhard Nessler, and Sepp Hochreiter. GANs Trained by a Two Time-Scale Update Rule Converge to a Local Nash Equilibrium. In *Advances in Neural Information Processing Systems*, pages 6626–6637, 2017.
- [167] Mehdi SM Sajjadi, Olivier Bachem, Mario Lucic, Olivier Bousquet, and Sylvain Gelly. Assessing Generative Models via Precision and Recall. In *Advances in Neural Information Processing Systems*, pages 5228–5237, 2018.
- [168] Anuj Srivastava. Stochastic models for capturing image variability. *IEEE Signal Processing Magazine*, 19(5):63–76, 2002.
- [169] Anuj Srivastava, Xiuwen Liu, and Ulf Grenander. Universal analytical forms for modeling image probabilities. *IEEE Transactions on Pattern Analysis and Machine Intelligence*, 24(9):1200–1214, 2002.
- [170] Jia Deng, Wei Dong, Richard Socher, Li-Jia Li, Kai Li, and Li Fei-Fei. Imagenet: A large-scale hierarchical image database. In *2009 IEEE Conference on Computer Vision and Pattern Recognition*, pages 248–255, 2009.
- [171] Christian Szegedy, Vincent Vanhoucke, Sergey Ioffe, Jon Shlens, and Zbigniew Wojna. Rethinking the Inception Architecture for Computer Vision. In *Proceedings of the IEEE conference on computer vision and pattern recognition*, pages 2818–2826, 2016.
- [172] Huai Geng Zheng. *Static and dynamic analysis of near infra-red dorsal hand vein images for biometric applications*. PhD thesis, University of Central Lancashire, 2017.